Heinrich Heine
Universität
Düsseldorf

The Effect of Natural Genetic Variation at *PPD-H1* on Shoot Apex Development in Response to High Ambient Temperature in Barley (*Hordeum vulgare* L.)

Inaugural dissertation

for the attainment of the title of doctor
in the Faculty of Mathematics and Natural Sciences
at the Heinrich Heine University Düsseldorf

presented by

Tianyu Lan
from Luoyang, China

Düsseldorf, October 2023

from the Institute for Plant Genetics
at the Heinrich Heine University Düsseldorf

Published by permission of the
Faculty of Mathematics and Natural Sciences at
Heinrich Heine University Düsseldorf

Supervisor: Prof. Dr. Maria von Korff Schmising
Co-supervisor: Prof. Dr. Rüdiger Simon

Date of the oral examination: 12.12.2023

Affidavit for the dissertation entitled:

The Effect of Natural Genetic Variation at *PPD-H1* on Shoot Apex Development in Response to High Ambient Temperature in Barley (*Hordeum vulgare* L.)

I declare under oath that I have produced my thesis independently and without any undue assistance by third parties under consideration of the 'Principles for the Safeguarding of Good Scientific Practice at Heinrich Heine University Düsseldorf'.

Place, date

Signature

Table of Contents

Summary

Global climate change threatens crop yields worldwide. Even small increases above the optimal growth temperatures impair spike development and fertility, thus significantly reducing the productivity of temperate cereal crops, such as barley (*Hordeum vulgare*) and wheat (*Triticum aestivum*). The photoperiod response gene, *PHOTOPERIOD1* (*PPD-H1*), is a major regulator of thermal-responsive flowering in barley. A recessive mutation in the CCT domain of *Ppd-H1* (*ppd-h1* allele) prevalent in spring barley delays flowering and causes a severe reduction in floret and grain number under high ambient temperature (HT). By contrast, introgressing the wild-type *Ppd-H1* allele from winter or wild barley genotypes to the spring barley accelerates reproductive development and maintains floret fertility and grain number under HT. However, the mechanisms underlying the interaction between *Ppd-H1* and ambient temperatures in regulating plant growth, spike development, and, thus, grain yield, are poorly understood. I investigated the effects of natural variation at *PPD-H1* on shoot growth and inflorescence development under HT and identified genes and regulatory networks in the leaf and main shoot apex (MSA) associated with HT- and *Ppd-H1*-dependent developmental changes in barley.

I used two spring barley cultivars, Golden Promise (GP) and Scarlett, with the mutant *ppd-h1* allele, and their derived near-isogenic lines (NILs), GP-fast and S42-IL107, carrying the wild-type *Ppd-H1* allele, to study the morphological and molecular changes in response to HT. Characterization of shoot growth revealed that HT reduced plant height and leaf width but increased leaf appearance rates (LAR) independent of *PPD-H1*. By contrast, HT reduced above-ground dry biomass and affected inflorescence and floral development in a *PPD-H1*-dependent manner. HT reduced the spikelet meristem (SM) and floral meristem (FM) induction rates but increased the duration of SM and FM induction in the parental lines. By contrast, HT increased the SM and FM induction rate but reduced the duration of SM and FM induction in the NILs. The final numbers of SMs and FMs were thus determined by the rate and duration of SM and FM induction, which were negatively correlated. Consequently, the final numbers of SMs and FMs did not strongly vary between control ambient temperatures (CT) and HT in all genotypes. The reduction in inflorescence meristem (IM) width was positively associated with the SM induction rate but negatively linked

to the duration of SM induction, suggesting that IM width declines as it provides founder cells for the SM on its flanks.

To examine whether HT impacted SM induction and number through modifying auxin homeostasis in the IM, I analyzed two auxin reporter lines, HvpPIN1a:HvPIN1a-mVENUS and DR5v2:VENUS-H2B, in the IM of GP and GP-fast. HT reduced the expression of the auxin efflux transporter HvPIN1a and the auxin indicator DR5v2 in the IM at the spikelet induction stage (W2.0) in all reporter lines, but these alterations were more pronounced in GP than in GP-fast. High levels of auxin in the IM have been associated with reduced IM maintenance and activity in *Arabidopsis thaliana*. Consequently, HT- and *Ppd-H1*-dependent changes in auxin concentrations in the IM might underlie the differences in the SM induction rate between genotypes and temperatures.

The HT- and *PPD-H1*-dependent changes in the final grain number were mainly caused by differences in floret fertility. Dissection of floral development showed that HT impaired anther development and pollen viability in the parental lines, which likely contributed to reduced fertility and grain number under HT. While HT effects were most pronounced at the floral development stage, the temperature-photoperiod co-shift experiment showed that the vegetative meristem was more susceptible to HT than the reproductive meristem. Furthermore, HT at the vegetative stage affected the development of SM and FM even several weeks after the transfer to CT, demonstrating that HT at the vegetative stage had a long-term effect on reproductive development and SM and FM induction.

To identify HT- and *PPD-H1*-dependent gene regulatory networks linked to the differential developmental responses to HT, I analyzed the global transcriptome changes in response to HT in leaves and MSAs at different developmental stages in all four genotypes. In both leaves and MSAs, the number of differentially expressed genes (DEGs) and the magnitude of expression changes were higher in the parental lines than in the NILs. The higher transcriptional plasticity of the parental lines was correlated with their higher phenotypic plasticity in response to HT compared to the NILs. HT caused the up-regulation of genes with functions in stress response and protein folding in both MSA and leaf. In contrast, HT caused a down-regulation of photosynthesis-related genes in the leaves and of chromatin remodeling genes in the MSA, particularly in the parental lines. Consequently, the moderate and long-term rise

in ambient temperature-induced expression changes in the parental lines are comparable to those observed under short-term heat stress. Analysis of genetic differences between parental lines and NILs confirmed that the majority of *Ppd-H1*-dependent genes under both CT and HT had functions in biotic and abiotic stress responses. *Ppd-H1* may thus play a crucial role in mitigating stress susceptibility, as demonstrated by the genetic differences in inflorescence development and grain set, as well as in gene expression and transcriptional plasticity in response to HT.

Under HT, the transcript levels of the flowering inducer *FLOWERING LOCUS T1* (*FT1*), the barley homolog of *FLOWERING LOCUS T* (*FT*) in Arabidopsis, was down-regulated in the leaf of all genotypes, except S42-IL107. The transcriptional changes of *FT1* were associated with floral developmental regulators, i.e., *FLOWERING LOCUS T*2 (*FT2*), *FLOWERING PROMOTING FACTOR-LIKE* gene (*FPFL*), and *BARLEY MADS-BOX 3* (*BM3*), and auxin signaling-related genes, i.e., *SRS TRANSCRIPTION FACTOR*, in the MSA. The genetic differences in floral development under HT correlated with the differential expression of many genes related to photosynthesis, carbohydrate and energy metabolism, and anther and pollen development in the MSA. These genes were significantly down-regulated in the parental lines but up-regulated or maintained in the NILs under HT, suggesting that the development of the photosynthetic apparatus in the spike might be important to ensure energy supply for floret fertility under HT.

Taken together, this study shows that *PPD-H1* interacts with HT to control the rate and duration of SM and FM induction and, thus, IM activity and maintenance. Furthermore, HT impairs floret fertility by impacting anther and pollen development in a genotype-specific manner, suggesting that *Ppd-H1* improves anther and pollen development under HT in barley. I could demonstrate that the vegetative MSA was more susceptible to HT treatment than the reproductive MSA, as seen by the long-term effects of HT on the SM and FM induction after transfer to CT. RNA-sequencing revealed that HT reduced the expression of floral inducers in the leaf and floral development regulators in the MSA. Differential expression of genes related to stress response, photosynthesis, and carbohydrate and energy metabolism suggested that the overall stress resistance, photosynthetic apparatus development, and energy metabolism may underly the *Ppd-H1*-dependent differences in floret fertility under HT. *PPD-H1* has been described as a key regulator of stress adaptation through its role in controlling flowering time and stress escape in agricultural regions with terminal stress. I could

demonstrate that in addition to stress escape, *PPD-H1* controls stress adaptation by modifying overall stress resistance, and thus floret fertility and grain set under HT.

1 Introduction

1.1 The Effect of Global Warming on Crop Productivity

Due to global climate change, major temperate crops, such as barley (*Hordeum vulgare*) and wheat (*Triticum aestivum*), are increasingly subjected to high ambient temperatures (HT): in 2022, the average global surface temperature was 0.86 °C warmer than the 20th-century average of 13.9 °C and is expected to rise even further until the end of the 21st century (IPCC, 2022). Small increases in the average ambient temperature above the optimal growth temperatures have strong adverse effects on crop yield. Field studies and model predictions have shown that each 1 °C increase in seasonal and global temperature can cause significant grain yield losses in wheat and barley (Tashiro and Wardlaw, 1989; Hakala et al., 2012; Ottman et al., 2012; Zhao et al., 2017; Xie et al., 2018). Barley is not only an essential crop as animal feed and the main ingredient of beer and whiskey production, but also an important crop model species to study the genetic underpinnings of agronomic traits and adaptation to abiotic stresses (Langridge, 2018). Understanding how barley reproductive development responses to HT and unraveling the genetic and molecular networks underlying the developmental thermal responses are crucial for breeding thermotolerant barley and wheat varieties for future climate challenges.

1.2 Morphological and Molecular Responses to Elevated Ambient Temperatures in Plants

HT below the heat-stress threshold induces a suite of morphological and architectural changes in plants collectively called thermomorphogenesis (Delker et al., 2022). In the model plant *Arabidopsis thaliana*, HT enhances the elongation of hypocotyls, stems, leaf petiole, and hyponasty but reduces leaf blade size (Casal and Balasubramanian, 2019). The longer hypocotyls could facilitate moving the sensitive shoot apex meristem of the seedling away from the hot soil, and the leaf hyponasty could decrease the midday solar radiation exposure and improve leaf cooling (Casal and Balasubramanian, 2019). In addition, HT accelerates flowering and overcomes the delay in flowering under short-day (SD) conditions through up-regulation of the florigen, *FLOWERING LOCUS T* (*FT*) transcript level in Arabidopsis (Balasubramanian et al., 2006). A bHLH transcription factor PHYTOCHROME-INTERACTING FACTOR 4 (PIF4) plays a key role in thermomorphogenesis by

orchestrating transcriptional changes that trigger primarily phytohormone-induced hypocotyl and petiole elongation responses by induction of *FT* transcription (Koini et al., 2009; Franklin et al., 2011; Kumar et al., 2012). Epigenetic modifications and chromatin remodeling play a prominent role in thermomorphogenesis, where HT decreases histone occupancy of DNA, thereby improving DNA accessibility and transcriptional activation or repression of thermomorphogenic genes and *FT* (Kumar et al., 2012; Huai et al., 2018; Van Der Woude et al., 2019). Moreover, exogenous application of plant growth regulators like auxin can mitigate HT-induced damage on anther and pollen development, thus improving fertility (Sakata et al., 2010).

While many of the phenotypic and molecular responses to HT are conserved across species, the temperate cereal crops barley and wheat display ambient temperature responses that are clearly distinct from those observed in Arabidopsis. For example, PIF4 does not seem to act as a major regulatory hub controlling growth and thermomorphogenesis in barley and wheat (Zhu et al., 2023).

1.3 Genetic Control of Flowering Time and Grain Set under High Ambient Temperature

In barley and wheat, HT reduces stem elongation, and plants become stunted and more compact with reduced plant height and total biomass (Batts et al., 1997; Hemming et al., 2012; Zhu et al., 2023). Furthermore, HT displays genotype-specific effects on reproductive development, either accelerating or delaying flowering in both species (Ejaz and von Korff, 2017; Dixon et al., 2019). Recent studies have identified the photoperiod response gene, *PHOTOPERIOD1* (*PPD-H1*), a barley homolog of *PSEUDO RESPONSE REGULATOR 37* (*PRR37*) in Arabidopsis, as a major regulator for thermal-responsive flowering (Ejaz and von Korff, 2017; Wiegmann et al., 2019; Gol et al., 2021). Originally, *PPD-H1* was identified as a photoperiod response gene that accelerates reproductive development under long-day (LD) conditions by up-regulating *FLOWERING LOCUS T1* (*FT1*), the barley homolog of *FT* in Arabidopsis, in the leaf (Digel et al., 2015). A natural mutation in the CCT domain of *Ppd-H1* (*ppd-h1* allele) prevalent in spring barley causes a reduction in *FT1* expression and a delay in flowering time under LD conditions (Turner et al., 2005). Ejaz and von Korff (2017) demonstrated that *PPD-H1* also controls flowering time in response to HT, where the wild-type *Ppd-H1* allele accelerates flowering under HT, but the natural *ppd-h1* mutant allele delays flowering under HT (Ejaz and von Korff, 2017). This allele-specific delay

in flowering time under HT was linked to reduced floret fertility and grain number. By contrast, genotypes with the wild-type *Ppd-H1* allele maintained high floret fertility and grain set under HT. Analysis of floral regulator genes in the leaf revealed that the transcript level of *FT1* was down-regulated by HT irrespective of the *PPD-H1* allele, which did not correlate with its accelerated flowering under HT. The down-regulation of *FT1* in the HT-induced flowering genotypes clearly differed from the effects observed in Arabidopsis, in which *FT* is strongly up-regulated by HT (Balasubramanian et al., 2006). These observations suggested that the genetic and molecular control of thermomorphogenesis differs between Arabidopsis and barley.

1.4 Thesis Aims

The aim of my study was thus to dissect the effects of *PPD-H1* on the shoot and different stages of inflorescence and floral development to identify critical developmental stages and traits that explain the *PPD-H1*-dependent differences in development and final grain set under HT. Furthermore, my objective was to identify *PPD-H1*-dependent genes and gene regulatory networks that underly the HT-induced changes in developmental timing and leaf and floral development in barley.

2 Results

2.1 High Ambient Temperature Affects Plant Development

To evaluate the interaction between ambient temperatures and *PPD-H1* alleles on plant growth and development, we characterized flowering time, shoot architecture traits, and inflorescence development in two pairs of near iso-genic lines (NILs), carrying different allelic variants for *PPD-H1* under control (CT; 20°C/16°C) and high ambient temperature (HT; 28°C/24°C). We used spring barley cultivar Golden Promise (GP), with the mutated *ppd-h1* allele, and its derived NIL, GP-fast, with the wild-type *Ppd-H1* allele from winter barley (Gol et al., 2021). The major phenotypic and molecular effects of *PPD-H1* in response to HT were confirmed in another spring barley cultivar Scarlett (*ppd-h1* allele), and its derived NIL S42-IL107 (*Ppd-H1* allele) (Ejaz and von Korff, 2017; Gol et al., 2021).

The flowering time of the spring barley genotypes, GP and Scarlett, was delayed compared to their respective NILs, GP-fast and S42-IL107, under CT and LD (16h/8h, day/night) conditions (Digel et al., 2015; Gol et al., 2021) (Figure 1A; Supplemental Figure S1A-B). However, HT further delayed flowering in the parental lines but accelerated the flowering in the NILs (Figure 1A; Supplemental Figure S1A-B). In addition, HT significantly reduced the plant height and above-ground dry biomass in all four genotypes, although the number of tillers and spikes was increased under HT in the parental lines (Figure 1B-E; Supplemental Figure S1C-F). Furthermore, the leaf appearance rate (LAR) on the main culm was higher in GP-fast than in GP under CT, which was positively associated with the flowering time (Figure 1A; Supplemental Figure S2A). However, HT led to an increase in LAR but delayed flowering in GP, whereas in GP-fast, HT accelerated both LAR and flowering compared to CT (Figure 1A; Supplemental Figure S2A). It suggests that the reproductive development and leaf growth were partly decoupled under HT, and this was dependent on genetic variations at *PPD-H1*. HT did not alter the number of leaves on the main culm in GP and GP-fast compared to CT, although the LAR was increased under HT (Supplemental Figure S2A-C). In both genotypes, the shape of leaves became longer and slimmer under HT as compared to CT, except for the last 1-3 leaves that were shorter and slimmer under HT than CT (Supplemental Figure S2B and C). A comparison of leaf cell size in the second leaf between CT and HT revealed that HT reduced the cell length and width in

both GP and GP-fast (Supplemental Figure S2D and E). Consequently, the elongation of the leaf blade under HT resulted from the increased cell number.

We further characterized the effect of HT on inflorescence development by dissecting the main shoot apex (MSA) of GP and GP-fast every three to five days and rating the developmental stage from seedling emergence to pollination according to the Waddington scale (Waddington et al., 1983) (Figure 1F and G). In both genotypes, HT caused a mild but significant delay in the MSA development from vegetative to spikelet induction (W0-W2.0) (Figure 1F). However, HT strongly delayed reproductive development (W2.0-W10.0) in GP but accelerated it in GP-fast compared to CT, resulting in a strong delay and acceleration in flowering time in GP and GP-fast, respectively, as already demonstrated for Scarlett and S42-IL107 (Figure 1A and G) (Ejaz and von Korff, 2017).

Taken together, the effects of HT on flowering time, tiller and spike numbers, above-ground dry biomass, and inflorescence development differed between parental lines and NILs, suggesting that *PPD-H1* interacted with HT to control shoot growth and spike development. By contrast, HT caused a relative reduction in plant height and altered the LAR and leaf blade shape independent of *PPD-H1*.

2.2 Ambient Temperature Interacts with *PPD-H1* to Regulate Spikelet Meristem and Floral Meristem Induction

Upon transition to reproductive growth, the indeterminate barley inflorescence meristem (IM) generates spikelet meristems (SMs) on its flanks, which then differentiate into floral meristems (FMs), and each develops into flowers (or florets) and grains. During the early reproductive phase, the IM of barley produces SM until the initiation of pistil primordia (W4.5). Typically, the duration of the spikelet induction phase, from the spikelet initiation (W2.0) to the presence of pistil primordium (W4.5) stage, is positively correlated with the final spikelet, floret, and grain numbers (Digel et al., 2015). Accordingly, the late-flowering genotypes GP and Scarlett generated more SMs and FMs on the MSA than the early-flowering genotypes GP-fast and S42-IL107 under both CT and HT (Figure 1H and I; Supplemental Figure S1G and H; T Supplemental able S1). However, HT prolonged the spikelet induction phase but did not increase the SM and the FM numbers in the parental lines compared to CT, whereas in the NILs, HT shortened the period of spikelet induction but maintained or

slightly reduced the SM and FM numbers compared to CT (Figure 1H and I; Supplemental Figure S1G and H; Supplemental Table S1).

To understand why the association between the duration of spikelet induction and SM number was changed under HT, we scored the rate of SM induction in all genotypes under CT and HT. HT reduced the rate of SM induction from 1.7 to 0.9 SMs/day in GP and from 2.3 to 1.3 SMs/day in Scarlett, but SM induction was accelerated by HT from 1.5 to 2.0 SMs/day in GP-fast and from 2.0 to 2.8 SMs/day in S42-IL107 between W2.0 and W3.5 (Supplemental Table S1). Since HT had opposing effects on the rate and duration of SM initiation, the final SM number was not strongly altered under HT compared to CT, neither in the parental lines nor the NILs (Supplemental Table S1). Moreover, the differences in SM induction rates in response to HT between W2.0 and W3.5 were correlated with the decline in the IM width; the higher the SM induction rates, the faster the IM width declined (Supplemental Figure S3; Supplemental Table S2). No correlation was observed between the IM height and SM induction rate (Supplemental Figure S3C; Supplemental Table S2). These observations suggested that the reduction in the IM width, but not height, was positively associated with the SM induction rate but negatively correlated with the duration of SM induction.

As observed for the SM, the number of final FMs was higher in the parental lines than in NILs under CT and HT conditions (Figure 1I; Supplemental Table S1). Similarly, the effect of HT on the FM induction rate was also observed during the spikelet induction phase in a genotype-specific manner (Figure 1I; Supplemental Table S1). Furthermore, HT strongly reduced the number of final florets and grains, and this reduction was more pronounced in the parental lines than in the NILs (Figure 2A-C; Supplemental Figure S4A-C). HT caused a strong floral abortion at the tip of inflorescence in the parental lines but not in the NILs; thus, the number of mature florets was significantly reduced in the parental lines compared to the NILs (Supplemental Figure S4E). While the floret number under HT was still higher in the parental lines than in the NILs, the final grain number was higher in the NILs than in the parental lines under HT, indicating that HT interacted with *PPD-H1* to control floret fertility (Figure 2D; Supplemental Figure S4D). We observed that HT reduced floret fertility at all node positions along the main inflorescence in all genotypes, while the impact was more pronounced in the parental lines than in the NILs, particularly at the tip and base of the spike (Supplemental Figure S4E). Consequently, HT caused a reduction of, on average, 20

grains in the parental lines but only five grains in the NILs on the MSA (Supplemental Table S1). In the parental lines, 50-60% of SMs developed into grains under CT, but only 11-15% of SMs developed into grains under HT (Supplemental Table S1). By contrast, in the NILs, HT only reduced the development of SM to grain from 58-61% to 50% (Supplemental Table S1).

To investigate the causes of floret sterility under HT in the parental lines, anther morphology and pollen viability of the central florets at the middle of the MSA were examined. We observed that under CT, the anthers were fully filled with yellow pollens and elongated above stigmatic branches at the pollination stage in all genotypes (Figure 2G). By contrast, under HT, the anther size in the parental lines was greatly reduced and the anthers were pale and empty, whereas in the NILs, the anther size was not affected in GP-fast and only slightly reduced in S42-IL107 under HT (Figure 2E; Supplemental Figure S4F). We confirmed with Alexander staining that the majority of pollen from the parental lines grown under HT were aborted, while no significant difference in pollen viability was observed in the NILs under different ambient temperatures (Figure 2F; Supplemental Figure S4G). Apart from the HT impact on the grain set, the grain shape and weight were also affected by HT (Figure 2H-I; Supplemental Figure S4H-L). Grain length was increased under HT in all genotypes compared to CT, whereas grain width was most prominently reduced in the parental lines, resulting in a reduction in the thousand-grain weight (TGW) of 25% in the parental lines while only 15% in the NILs under HT compared to CT (Figure 2H-I; Supplemental Figure S4H-L).

Taken together, HT affected SM induction rate and duration, anther and pollen development, floret fertility, and grain development in a genotype-specific manner, suggesting that *PPD-H1* interacted with ambient temperature to regulate developmental processes at different reproductive stages.

2.3 High Ambient Temperature Affects the Activity and Maintenance of Inflorescence Meristem and Floral Meristem at the Early Developmental Stage

HT had the strongest effects on floral development at the late reproductive phase (W6.0). We thus decided to test: a) if the MSA was more sensitive or responsive to HT at the floral developmental stage (W6.0) than at the vegetative and early reproductive stages (W1.0-W3.5) or b) if the translation of the HT impacts into a

phenotypic change was added up over time, thus becoming more apparent at the late reproductive stage. Since the SM induction rate declined rapidly with the onset of FM differentiation, and FM differentiation but not SM induction is largely LD-dependent, we thus performed a photoperiod-temperature co-shift experiment (Figure 3A). We grew GP and GP-fast plants under LD (16h/8h, light/dark) at CT until W2.0 and then shifted the plants to SD (10h/14h, light/dark) at either CT (CC) or HT (CH). Likewise, GP and GP-fast plants grown under LD at HT until W2.0 were shifted to either CT (HC) or HT (HH) (Figure 3A). Under SD, SMs are initiated while the differentiation of FM into florets is repressed (Digel et al., 2015). We thus tested the effects of HT on SM and FM induction in the absence of floret development.

HT delayed SM and FM induction in GP but accelerated SM and FM induction in GP-fast as observed in the experiment under constant LD (Figure 3B-D). The effect of HT on SM and FM induction rates was most pronounced when applied before spikelet induction (W2.0) (Figure 3C and D). The effect of HT before and after spikelet induction (W2.0) was additive and consequently most pronounced under HH, followed by HC and CH (Figure 3C and D). In addition, HT affected the shape of the inflorescence in GP under HH and HC, resulting in an inflorescence with the most advanced FMs at the base and a large number of undeveloped SMs on the apical part (Figure 3B). It suggests that HT before spikelet induction (W2.0) repressed FM development in GP. By contrast, in GP-fast, the SMs developed into FMs along the entire inflorescence under HH and HC (Figure 3B and D). The spike shape clearly differed from the typical lanceolate shape (Bonnett, 1966), where the florets at the central spike are more advanced in development compared to those at the basal and distal parts (Figure 3B). Moreover, we observed floral reversion, with FM reversed to IM in GP under HT before and after spikelet induction (HH) but not under other conditions and genotype combinations (Supplemental Figure S5).

In barley, SHORT VEGETATIVE PHASE (SVP) family MADS-box transcription factors, BM1, BM10, and VRT2, and CENTRORADIALIS (CEN) function as flowering repressors and negatively regulate IM activity (Trevaskis et al., 2007; Bi et al., 2019). In MSA samples collected at 32 days for GP and 22 days for GP-fast after the shift to SD, the expression of *BM1*, *BM10*, *VRT2,* and *CEN* were most strongly up-regulated in GP but most strongly down-regulated in GP-fast in HH, followed by HC, CH, and CC (Figure 3E-H). The transcriptional changes of these genes were associated with

the observed differences in SM and FM induction rates, inflorescence shape, and floral reversion.

Taken together, the MSA could sense and translate temperature signals before spikelet induction (W2.0) to control later SM and FM development. Expression patterns of *SVP-LIKE* genes and *CEN* in MSAs correlated with genotype- and temperature-dependent differences in SM induction rate and FM development.

2.4 Characterization of Transcriptional Changes in Temperature- and *PPD-H1*-dependent Genes in Leaves

To identify molecular changes responsible for the *PPD-H1*-dependent differences in development, floret fertility, and grain set in response to HT, we investigated the changes in global leaf and MSA transcriptomes in response to HT. We harvested the latest fully elongated leaves and MSAs of GP and GP-fast under CT and HT conditions at four developmental stages: the vegetative (W1.0), spikelet induction (W2.0), stamen primordium (W3.5), and style primordium (W6.0) stages. To confirm the major effects of *PPD-H1* and HT on leaf and MSA transcriptome, we harvested the same tissues of Scarlett and S42-IL107 at the stamen primordium (W3.5) and style primordium (W6.0) stages under both temperature conditions.

A principal component analysis (PCA) of leaf samples revealed that temperature differences explained most of the variations in the transcriptomes, while the developmental stage had a minor effect (Supplemental Figure S6A-B). We, thus, filtered for genes regulated by ambient temperature in each genotype in at least three out of four developmental stages ($|\log_2 FC| \geq 1$, FDR < 0.01, *ANOVA.p.temperature* < 0.01) (Table S3). In the leaf, we detected 870 differentially expressed genes (DEGs) in response to HT in GP, but only 497 DEGs in GP-fast (Figure 4A). Among them, 695 DEGs of GP and 362 DEGs of GP-fast exhibited similar temperature responses in Scarlett and S42-IL107 (Supplemental Figure S6C and D). A much greater number of genes were up-regulated by HT than down-regulated, particularly in GP and Scarlett, and these genes were enriched in stress response, protein folding, and chloroplast development pathways (Figure 4C; Supplemental Figure S6E; Supplemental Table S4). Particularly, genes involved in stress response and protein folding were more strongly up-regulated under HT in parental lines than in NILs, i.e., *HEAT SHOCK PROTEIN* genes (*HSPs*; *BART1_0-p37203*, *BART1_0-p47078*), and ROS scavengers

SUPEROXIDE DISMUTASE (*BART1_0-p48903*) and *THIOREDOXIN* (*BART1_0-p26987*) (Figure 4C and 4E, 5A-D; Supplemental Table S4). By contrast, down-regulated genes in response to HT were enriched in the photosynthesis pathway in all genotypes, i.e., genes encoding CHLOROPHYLL A-B BINDING (CAB) proteins (BART1_0-p38017, BART1_0-p06201), which control light uptake and energy flow between photosystems (Figure 4C and 4E, 5E and F; Supplemental Table S4).

Notably, *FT1*, the flowering inducer acting downstream of *PPD-H1*, was down-regulated by HT in leaves of all genotypes except S42-IL107 (Figure 4E, 5G). However, the transcript level of *FT1* was higher or equally high in the NILs under HT compared to the parental lines under CT (Figure 4E, 5G). Likewise, the putative *FT1* downstream targets *MADS-BOX* genes, *VRN1* (*BART1_0-p39106*) and *BM3* (*BART1_0-p57667*), were also down-regulated by HT and exhibited higher expression levels in the NILs under HT compared to the parental lines under CT (Figure 5H and I). By contrast, the putative flowering repressors, i.e., *FT4* (*BART1_0-p08722*) and the *FLOWERING PROMOTING FACTOR LIKE* genes (*FPFL*; *BART1_0-p07358*, *BART1_0-p07381*), were up-regulated in response to HT, particularly at the vegetative and early reproductive stages with the strongest impact in the parental lines compared to the NILs (Figure 5J-L). These results indicate that the overall higher transcriptional plasticity of the parental lines in response to HT included a stronger thermo-responsiveness of developmental genes compared to the NILs.

Moreover, about half of the ambient temperature-regulated genes exhibited a significant genotype×temperature interaction, where HT more strongly altered genes in the parental lines than the NILs (Supplemental Table S3). This prompted us to test for *PPD-H1*-regulated genes in the leaf under CT and HT. We identified 478 *PPD-H1*-regulated DEGs shared between two pairs of the NILs under CT, of which 364 DEGs had higher expression levels in the parental lines than in the NILs (Supplemental Table S3). Likewise, under HT, there were 329 *PPD-H1*-regulated DEGs shared between two pairs of NILs, of which 246 DEGs were higher expressed in the parental lines than in the NILs (Supplemental Table S3). Notably, the majority of genes that were higher expressed in the parental lines than NILs, function in biotic and abiotic stress signaling and response, calcium ion binding, and protein phosphorylation, i.e., *WRKY* transcription factor genes, *CYSTINE-RICH-RECEPTOR-LIKE KINASE* genes (*CRKs*), *WALL-ASSOCIATED KINASE* genes (*WAKs*) and *CALRETICULIN/CALNEXIN* (Supplemental Table S5). Compared to the NILs, the stronger transcriptional changes

observed in the leaf of the parental lines, along with their higher transcript levels of stress-related genes, indicated that the wild-type *Ppd-H1* allele acts as a repressor of stress-related genes in the leaf, thus contributing to cellular homeostasis maintenance under HT (Supplemental Table S5). In addition, the higher transcript levels of stress signaling and stress response-related genes in the parental lines were in line with the higher floret abortion under CT and HT compared to the NILs (Supplemental Table S5). We thus investigated transcriptome changes in the MSA to identify genes correlated with the *PPD-H1*-dependent developmental differences in response to HT.

2.5 Characterization of Transcriptional Changes in Temperature- and *PPD-H1*-dependent Genes in Main Shoot Apices

The PCA of the MSA transcriptome in the parental lines and the NILs at different temperatures and developmental stages revealed that in contrast to the leaf transcriptome, the MSA samples showed a clear separation by the developmental stage, while the ambient temperature only clearly differentiated the transcriptomes of the parental lines, not the NILs (Supplemental Figure S7A and B). In addition, the MSA transcriptome significantly differed between the early (W1.0-W3.5) and the late (W6.0) developmental stages, which was associated with the profound morphological differentiation of the inflorescence during floret development (Supplemental Figure S7A and B). We, therefore, analyzed the temperature response of MSA samples at the vegetative and early reproductive stages (W1.0-W3.5) together, separately from those at the late reproductive stage (W6.0). As the developmental stage had a strong effect on the MSA transcriptome, we filtered for genes regulated by ambient temperature in at least one of the developmental stages ($|\log_2 FC| \geq 1$, FDR < 0.01, *ANOVA.p.temperature* < 0.01) (Supplemental Table S6). As seen in the leaf transcriptome, a much greater number of genes were differentially regulated by HT in the parental lines than in the NILs (Figure 4B). In the MSA at the early developmental stage (W1.0-3.5), we detected 1273 DEGs in GP and 926 DEGs in Scarlett, but only 548 DEGs in GP-fast and 524 DEGs in S42-IL107 (Figure 4B; Supplemental Figure S7C and D). At floret development (W6.0), we detected 6752 DEGs in GP and 889 DEGs in Scarlett, but only 1436 and 498 DEGs in GP-fast and S42-IL107, respectively (Figure 4B; Supplemental Figure S7C and D). Furthermore, up-regulated genes in response to HT were enriched for heat response, protein folding, and ubiquitination pathways, while down-regulated genes were involved in cell cycle control and

chromatin remodeling, particularly in the parental lines (Figure 4D; Supplemental Figure S7E, S8A; Supplemental Table S4). As in the leaf, over half of the DEGs also showed a genotype×temperature interaction in the MSA (Supplemental Table S6). For example, *HSPs* (*BART1_0-p37203*, *BART1_0-p47078*) and genes catalyzing redox reaction, i.e., *ALDO/KETO REDUCTASE* (*BART1_0-p30221*) and *ALPHA-KETOGLUTARATE-DEPENDENT DIOXYGENASE ALKB* (*BART1_0-p40418*), showed a stronger up-regulation under HT in the parental lines than in the NILs (Figure 4E, 6A-D). Notably, a number of *HSP20* genes were explicitly expressed at W6.0 and down-regulated in the parental lines but up-regulated in the NILs (Supplemental Figure S8B). By contrast, histone variants, notably *H2A.Z* (*BART1_0-42487*, *BART1_0-42106*), homologs of *HTA8* in Arabidopsis, involved in chromatin condensation and thus gene expression regulation, were more strongly down-regulated in the parental lines in response to HT than the NILs (Figure 4D and E, 6E and F). Similarly, genes involved in cell cycle and division regulation, i.e., *CYCLINS* (*BART1_0-p14114*, *BART1_0-p22723*), were more strongly down-regulated in parental lines than NILs, especially at floret development (W3.5-6.0) (Figure 4E, 6G and H). These results suggested that, as in the leaf, HT had a genotype-specific effect on the MSA transcriptome, where the parental lines with a mutant *ppd-h1* allele were characterized by higher transcriptional plasticity in response to HT.

Next, we tested if there were also genotype-specific differences in the expression levels in the MSA, as observed in the leaf. In contrast to leaf, under CT, the majority of genes showed higher expression levels in the NILs (914 DEGs) than in the parental lines (532 DEGs) (Supplemental Table S6). However, under HT, more genes were expressed higher in the parental lines (1509 DEGs) than in the NILs (1286 DEGs) (Supplemental Table S6). Genes higher expressed in the NILs under both CT and HT were enriched for functions in photosynthesis, light response, chloroplast development, carbohydrate metabolism, and chromatin remodeling (Supplemental Table S5). The expression levels of *FT2* (*BART1_0-p19119*) and floral homeotic genes, like *BM8* (*BART1_0-p11618*), *MADS5* (*BART1_0-p50282*), as well as *MADS34* (*BART1_0-p39078*), were higher expressed in the MSA of the NILs compared to parental lines under CT and/or HT (Figure 4E; Supplemental Table S5). By contrast, genes higher expressed in the parental lines under CT and HT were primarily linked to ribosome biogenesis, protein degradation, gene silencing, and chromatin remodeling (Supplemental Table S5). Taken together, under CT and HT, *Ppd-H1* repressed the

transcript levels of stress-related genes in the leaf but elevated the photosynthesis, carbohydrate metabolism, chromatin remodeling, and floral development-related genes in the MSA.

2.6 Characterization of Transcriptional Changes in Development-, Temperature- and *PPD-H1*-dependent Genes in Main Shoot Apices

To further identify the candidate genes regulating *PPD-H1*-dependent differences in SM induction and floret development in response to HT, we focused our further analyses on temperature-regulated genes, which were also differentially expressed during the early MSA development (W1.0-W3.5) and floral development (W6.0). During W1.0 to W3.5, we identified 285 DEGs in GP and 132 DEGs in GP-fast that were regulated by both ambient temperature and developmental stage. At W6.0, 3222 DEGs in GP and Scarlett and 401 DEGs in GP-fast and S42-IL107 were regulated by ambient temperature (Figure 7A and B; Supplemental Table S6). These genes were significantly involved in development, hormone signaling, carbohydrate assimilation, and metabolism (Figure 7C). In accordance with the differential down-regulation of *FT1* by HT in the leaf, genes regulating stem cell maintenance and floral development showed a strong down-regulation in response to HT in the MSA (Figure 7D-I). This effect was more pronounced in the parental lines than in the NILs (Figure 7D-I). For example, stem cell maintenance genes, i.e., the receptor kinase-like gene *LRR-RLK* (*BART1_0-p06909*), *CEN* (*BART1_0-p12251*), and *ALOG* transcription factor gene (*BART1_0-p56044*), were down-regulated at W1.0-W2.0, and floral developmental regulators, i.e., *FT2* (*BART1_0-p19119*), another homolog of *FT* which expressed in the MSA, *FPFL* gene (*BART1_0-p07358*), and *BM3* (Figure 7D-I), which are predominantly expressed in the differentiating floral organs, the main inflorescence vasculature, and the pedicel secondary vasculature, were down-regulated by HT at W3.5 especially in parental lines (Figure 7J-K). Furthermore, genes involved in phytohormone biosynthesis and signaling were co-regulated by HT with these floral developmental regulators (Figure 7C and L-N). For example, at W3.5, the auxin biosynthetic and signaling genes, *SRS* transcription factor (*BART1_0-p55105*), was down-regulated in the MSA under HT, whereas *SMALL AUXIN-UPREGULATED RNA-LIKE* gene (*SAUR-LIKE*; *BART1_0-p13720*) and *DORMANCY/AUXIN ASSOCIATED* gene (*DRM/ARP*; *BART1_0-p26935*) were up-regulated in the MSA under HT (Figure 7L-N). The stronger expression changes of these genes in the parental lines than in

the NILs suggest that the *PPD-H1*-dependent differences on SM and FM induction might be associated with the thermal responsiveness of the genes functioning in stem cell maintenance, floral development, and auxin signaling and biosynthetic in the MSA.

Furthermore, a large number of genes related to carbohydrate metabolism, fixation, and transport were also co-regulated by development and ambient temperature in the MSA (Figure 7C, and O-R). For example, HT down-regulated genes involved in carbohydrate metabolism and fixation, i.e., *CARBOHYDRATE KINASE PFKB* gene (*BART1_0-p26715*) and *RIBULOSE BISPHOSPHATE CARBOXYLASE SMALL CHAIN 1A* genes (*RBCS1As*; *BART1_0-p34490, BART1_0-p34828*, *BART1_0-p35662*), in both parental lines and NILs (Figure 7O-R). However, the transcript levels of these genes were much higher in the NILs than in the parental lines, not only under CT but also under HT (Figure 7O-R). Interestingly, at floret development (W6.0), genes involved in photosynthesis were significantly down-regulated in response to HT in the MSA of the parental lines but were either up-regulated or maintained in the MSA of the NILs (Supplemental Figure S8). Similarly, genes involved in carbohydrate transport, i.e., *SUGARS WILL EVENTUALLY BE EXPORTED TRANSPORTER* (*SWEET*; *BART1_0-p26197*), *LEUCINE-RICH REPEAT EXTENSIN* genes (*LRXs*; *BART1_0-p26226*, *BART1_0-p26227*), *TREHALOSE 6-PHOSPHATE PHOSPHATASE* (*TPP*; *BART1_0-p09193*), and sucrose cleavage genes, i.e., *BETA-FRUCTOFURANOSIDASES* (*BART1_0-p42717*, *BART1_0-p41424*, *BART1_0-p48227*), which hydrolyze sucrose into glucose and fructose for sink utilization, were significantly down-regulated in the parent lines but up-regulated or not altered in the NILs under HT (Supplemental Figure S8B). Moreover, we found that HT more strongly down-regulated genes involved in meiosis and mitosis processes and in sexual organ development in the parental lines compared to the NILs at W6.0 (Supplemental Figure S8B). These included the male gametophytic regulator *JASON* (*BART1_0-p43641*), the mitotic spindle checkpoint protein gene *BUBR1* (*BART1_0-p44076*), the meiosis protein gene *SWITCH1* (*BART1_0-p38779*), the meiotic nuclear division regulator (*BART1_0-p45115*), the *REPLICATION PROTEIN* gene (*BART1_0-p30440*) (Supplemental Figure S8B), *bHLH89* transcription factor gene (*BART1_0-p50211*), and the pollen tube growth regulators (*BART1_0-p05415*, BART1_0-p51547, *BART1_0-p43947*, *BART1_0-p56175*) (Supplemental Figure S8B). By contrast, a negative regulator of ovule development, the *MADS-BOX* gene *BART1_0-p43019*,

was more strongly up-regulated by HT in parental lines compared to NILs (Supplemental Figure S8B).

Consequently, the transcript levels of carbohydrate metabolism, fixation, and transport were significantly higher in the MSA of the NILs than the parental lines under both CT and HT, suggesting that *Ppd-H1* may sustain carbohydrate utilization during floral development to maintain sink strength and protect floret fertility under HT.

In summary, the global transcriptome analyses conducted in both leaf and MSA suggest a pivotal role of *PPD-H1* in orchestrating essential cellular processes to maintain cellular homeostasis and enhance stress resistance and carbohydrate utilization. This regulatory function of *PPD-H1* is strongly linked to *PPD-H1*-dependent transcriptional changes in genes functioning in stem cell maintenance, floral development, auxin signaling, and carbohydrate assimilation and metabolism.

2.7 Auxin Transport and Concentration are Affected by High Ambient Temperature in Inflorescence Meristem

The IM coordinates the formation and polarity of lateral organs depending on auxin transport (Reinhardt et al., 2000; Heisler et al., 2005; Yamaguchi et al., 2013). Transcriptomic analyses in the MSA at the spikelet induction stage (W2.0) revealed that genes involved in auxin signaling were more dysregulated by HT in the parental lines compared to the NILs. To examine whether auxin homeostasis in the IM was affected by HT, we used two auxin reporter lines, HvpPIN1a:HvPIN1a-mVENUS and DR5v2:VENUS-H2B (Kirschner et al., 2018) in both GP and in GP-fast backgrounds to analyze the expression changes of auxin efflux transporter HvPIN1a and auxin indicator DR5v2 in the IM at W2.0. At the spikelet induction stage (W2.0), DR5v2:VENUS-H2B and HvpPIN1a:HvPIN1a-mVENUS were expressed predominantly in the IM, in the cells adjacent to the incipient SMs, the leaf ridge, and the main vasculature. DR5v2:VENUS-H2B was localized in the nuclei as driven by the histone H2B, while HvpPIN1a:HvPIN1a-mVENUS was predominantly localized in the plasma membrane (Figure 8A and B). HT caused a strong increase in the expression of DR5v2:VENUS-H2B in the center of the IM in both GP and GP-fast (Figure 8 C-F). Conversely, there was a reduction in the HvpPIN1a:HvPIN1a-mVENUS expression in the IM and in the main vasculature in both genotypes, but the reduction was more pronounced in GP than in GP-fast (Figure 8 G-J). These results indicated that auxin

transport and local concentration in the IM were affected by HT in a *PPD-H1*-dependent manner. Thus, *Ppd-H1* may maintain auxin homeostasis in the IM at the spikelet induction stage (W2.0), thereby preserving IM activity under HT.

3 Discussion

Warm ambient temperatures pose a significant threat to crop productivity and food security, particularly for temperate cereal crops like barley and wheat (Lobell et al., 2011; Liu et al., 2016; Ejaz and von Korff, 2017). This study dissects the effect of HT on the morphological and molecular responses in barley and explores the role of *PPD-H1* in mitigating the adverse impacts of HT on growth and development. For this purpose, we analyzed two pairs of spring barley genotypes with a mutant *ppd-h1* allele and their derived NILs with a wild-type *Ppd-H1* allele. To test the effects of natural variation at *PPD-H1* on HT responses, we selected NILs in different parental backgrounds with introgressions of the same *Ppd-H1* allele but from different donors. While we endeavored to minimize genetic similarities among the introgressions of the NILs, we cannot completely eliminate the possibility that other consistent genetic variants within the introgressions may have had an impact on the observed phenotypes.

3.1 High Ambient Temperature-Induced Shoot and Spike Developmental Changes in Barley

HT led to longer and slimmer leaves in both GP and GP-fast, thus independent of *PPD-H1* (Supplemental Figure S2). These alterations in leaf shape were reminiscent of the high temperature-induced petiole elongation in Arabidopsis (van Zanten et al., 2009). In addition, thermomorphogenic responses in Arabidopsis include marked hypocotyl elongation and leaf elevation (Gray et al., 1998; Crawford et al., 2012). These responses could enhance leaf cooling and shade avoidance (Casal and Balasubramanian, 2019). Thus, the molecular responses of leaf development to HT are largely conserved between dicots and monocots (Nelissen et al., 2016). In barley, HT accelerated leaf appearance but reduced stem elongation and final plant height, resulting in a more compact plant architecture (Figure 1; Supplemental Figure S2). A decrease in plant height under HT due to reduced internode elongation has previously been documented in both barley and wheat (Hemming et al., 2012; Abou-Elwafa and Amein, 2016; Kiss et al., 2017; Zhu et al., 2023). Stem elongation, which is closely linked to reproductive development in barley and wheat, exhibited a different response to HT compared to Arabidopsis. Moreover, changes in reproductive development under HT significantly varied among different barley genotypes and thus were genotype-specific.

Reproductive development and flowering time under HT were delayed in the parental lines but accelerated in the NILs (Figure 1). These observations suggest that *PPD-H1* interacts with high ambient temperature to control reproductive development and flowering time (Ejaz and von Korff, 2017). We dissected the timing of different developmental stages and tracked the development of MSA under CT and HT to identify the critical stages for the final floret and grain numbers. Under CT, the spikelet induction phase (W2.0-3.5) was positively correlated with the number of SMs and, thus, the number of florets and grains (Digel et al., 2015) (Figure 1 and 2; Supplemental Table S1). Under HT, the rate of SM induction was reduced, but the duration of the spikelet induction phase was extended in the parental lines (Figure 1; Supplemental Table S1). By contrast, in the NILs, HT accelerated the rate of SM induction but reduced its duration. As a result, the final numbers of SMs and FMs were not strongly affected between CT and HT in the parental lines and NILs (Figure 1; Supplemental Table S1). Therefore, the final numbers of SMs and FMs were determined by the rate and duration of SM induction, which were negatively correlated. This observation aligns with the IM activity, which is regulated by the phytohormone auxin. In Arabidopsis, auxin negatively regulates meristem activity in the shoot apical meristem (SAM) (Zhao et al., 2017; Shi et al., 2018). We found that HT induced auxin accumulation in the IM in both genotypes, implying the reduction in IM activity, as seen in the reduction in SM number under HT at W6.0 in both GP and GP-fast (Figure 8; Supplemental Table S1). Auxin accumulation in the IM might result from the interruption of auxin transport in the IM under HT. We showed that HT reduced the expression of HvpPIN1a:HvPIN1a-mVENUS in the IM of both genotypes, but the impact was more pronounced in GP than in GP-fast (Figure 8). As PINs direct auxin to the sites where new organs are being formed (Reinhardt et al., 2000; Heisler et al., 2005), the stronger reduction of HvpPIN1a:HvPIN1a-mVENUS may link to the slower rate of SM induction in GP under HT (Figure 8). However, we did not observe the opposite effect of HT on HvpPIN1a:HvPIN1a-mVENUS in the IM of GP-fast, as its SM induction was accelerated.

In rice and maize, the number of primary branches or SMs is positively associated with the size of the undifferentiated IM (Chu et al., 2006; Suzaki et al., 2006; Bommert et al., 2013; Bommert and Whipple, 2018; Li et al., 2022). Wang et al, 2023 have recently shown that in barley, IM width is negatively correlated with SM number and suggested that the wider IM in barley may repress spike elongation and limit spikelet formation

(Wang et al., 2023). We showed that the SM induction rate was positively correlated with the reduction in IM width (Supplemental Table S2). In GP, HT reduced the rate of SM initiation, and IM width remained relatively stable and more extensive compared to CT (Supplemental Table S2). In GP-fast, HT accelerated SM induction, and IM width declined more rapidly compared to CT (Supplemental Table S2). We thus conclude that IM width declines during the spikelet induction phase as it provides founder cells for SM on its flanks. Although HT had strong and opposing effects on IM activity and SM induction rate between the parental lines and the NILs, these effects did not strongly influence the final SM and FM numbers.

The major differences in final grain number were caused by genotype-specific impacts of HT on floral development and floret fertility (Figure 2; Supplemental Figure S4). Of all developmental stages, the timing of floral development was most strongly affected by HT, which was delayed in the parental lines and accelerated in the NILs (Figure 1). However, the temperature-photoperiod co-shift experiment showed that the early stages before spikelet induction (W2.0) were most susceptible to HT. Interestingly, HT before spikelet induction strongly affected SM and FM induction even 3-4 weeks after the shift to the CT condition (Figure 3). Moreover, the *PPD-H1*-dependent effect of HT on SM and FM induction rates was more pronounced when the plants were exposed to HT before spikelet induction than after (Figure 3). These observations imply that vegetative SAMs are most susceptible to HT, but the phenotypic consequences are most apparent at later stages of SM and FM development. Therefore, HT has a long-term effect on SM and FM induction, even when they are newly formed after HT exposure (Figure 3). This long-term effect of HT on floral development was associated with changes in spike shape and differential expression of *SVP-LIKE* genes *BM1*, *BM10*, and *VRT2*, in the MSA (Figure 3). Elevated expression levels of *SVP-LIKE* genes in GP under HT imply the suppression of SM and FM induction and floral development, which have previously been shown to be linked to floral reversion, spike branching, as well as floret abortion in wheat and barley (Trevaskis et al., 2007; Backhaus et al., 2022).

It has already been reported that the wild-type *Ppd-H1* allele improved floret fertility and grain set under HT (Ejaz and von Korff, 2017; Zhu et al., 2023). We further demonstrate that impaired anther development and pollen viability contribute to floret sterility in the parental lines, while they were not strongly affected by HT in the NILs (Figure 2; Supplemental Figure S4). We thus conclude that *Ppd-H1* plays an important

role in preserving anther and pollen development, thus maintaining floret fertility and grain number per spike under HT. Furthermore, the HT-induced decrease in grain number and delay in reproductive development altered the ratio of vegetative to reproductive biomass, thus impacting the source-sink relationship. Under CT, delayed reproductive development in the parental lines was positively correlated with the number of leaves (on the main culm), tillers, spikes, and grains (on the main culm) and thus with the overall above-ground dry biomass (Figures 1 and 2; Supplemental Figures S1 and S4). However, HT further delayed reproductive development and increased vegetative biomass, which did not translate into a higher grain set in the parental lines (Figures 1 and 2; Supplemental Figures S1 and S4). The vegetative biomass was thus not positively correlated with grain yield under HT, possibly due to the impaired inflorescence development or alterations in carbon assimilation and allocation. However, this impact is mitigated by introgressing the wild-type *Ppd-H1* allele. The NILs were able to maintain grain set and thus source-sink relationships under HT.

3.2 *Ppd-H1* Maintains Transcriptome Stability in Response to High Ambient Temperature

We aimed to identify HT- and *PPD-H1*-dependent molecular networks in the leaf and MSA linked to differential developmental responses of the parental lines and the NILs to HT. In both leaf and MSA, the number of DEGs and the magnitude of expression changes in response to HT were much higher in the parental lines than in the NILs (Figure 4). Consequently, the parental lines exhibited higher transcriptional plasticity, which was correlated with their higher phenotypic plasticity in response to HT.

Although plants were subjected to a moderate increase in the ambient temperature throughout their entire growth cycle, thus allowing for acclimation, the majority of up-regulated genes in the leaf and MSA were enriched in functions related to stress response and protein folding (Figure 4; Supplemental Figures S6 and S7). We observed a strong up-regulation of *HSPs* and *HEAT SHOCK TRANSCRIPTION FACTOR* genes (*HSFs*), ROS scavenger genes, and detoxification protein genes in the leaf and MSA under HT and down-regulation of photosynthesis-related genes in the leaf under HT (Figures 4 and 6; Supplemental Figure S7). These transcriptional changes strongly resemble those observed under conditions of short-term heat stress

in leaves and panicles of barley (Abiko et al., 2005; Mahalingam et al., 2022; Mikołajczak et al., 2023), *Brachypodium* (Liu et al., 2015), wheat (Qin et al., 2008; Liu et al., 2015), and rice (Zhang et al., 2012; Zhang et al., 2013). Furthermore, transcriptional changes in stress response-related genes were much more substantial in the parental lines than in the NILs. This correlated with the more severe stress phenotypes observed in the parental lines under HT, as seen in floret abortion (Figure 4). We thus concluded that the stronger transcriptional reprogramming in response to HT indicated the overall higher stress susceptibility in the parental lines compared to the NILs. Therefore, we hypothesized that the impaired spike development in the parental lines may result from their higher stress susceptibility rather than only from the transcriptional regulation of developmental genes by HT and *Ppd-H1*. To support our hypothesis, we analyzed genotype-dependent differences in the leaf transcriptomes under CT and HT, respectively. Interestingly, not only under HT but also under CT, DEGs between the parental lines and the NILs were primarily associated with biotic and abiotic stress signaling and response, and these genes exhibited higher transcript levels in the parental lines than the NILs in both CT and HT (Supplemental Table S5). *PPD-H1* is homologous to *PESUDO RESPONSE REGULATOR* genes from the circadian clock in Arabidopsis, which acts as transcriptional repressors of light signaling and stress response in a time-of-the-day specific manner (Liu et al., 2013; Yang et al., 2021). While the natural mutation in the CCT domain of *Ppd-H1* (*ppd-h1* allele) does not alter the diurnal and circadian expression of clock genes in barley (Gol et al., 2021), our findings suggest that *Ppd-H1* may control the expression of stress response-related genes, either directly or indirectly, and thus leading to the stress phenotypes that have been demonstrated for the abiotic stresses in barley and wheat (Ejaz and von Korff, 2017; Kiss et al., 2017; Gol et al., 2021).

One of the genes consistently regulated in the leaf between the parental lines and the NILs under HT was the flowering inducer *FT1*, a known target of *PPD-H1* (Turner et al., 2005; Digel et al., 2015). Higher levels of *FT1* in the leaf of the NILs under both CT and HT were positively correlated with higher expression levels of the floral developmental regulators (*FT2* and *FPFL*) and floral homeotic genes (*BM8*, *MADS5*, and *MADS34*) in the MSA as compared to the parental lines (Figures 4 and 7; Supplemental Table S6). However, the expression of *FT1* in the leaf and of floral development regulators in the MSA was down-regulated in all genotypes under HT,

which was not associated with the acceleration of reproductive development in the NILs under HT compared to CT (Figures 1, 4, and 7; Supplemental Table S6). This finding is in contrast to Arabidopsis, where HT accelerates flowering by up-regulating *FT* and the downstream floral homeotic genes (Balasubramanian et al., 2006). We did not identify any genes with expression patterns that correlated with the *PPD-H1*-dependent differences in the SM and FM induction in response to HT, including the *SVP-LIKE* genes detected in the temperature-photoperiod co-shift experiment. This might be the consequence of sampling MSAs of the parental lines and the NILs at the same developmental stage, thereby correcting for transcriptional differences closely correlated to the developmental stage of the MSA.

However, at floret development (W6.0), we observed many genes in the MSA related to photosynthesis, carbohydrate, and energy metabolism, as well as sexual organ development. The transcript levels of photosynthesis and carbohydrate metabolism-related genes that were down-regulated in response to HT in the parental lines were maintained or up-regulated in the NILs (Supplemental Figure S8). It has been recently shown that the disruption of spike greening is linked to floral abortion and anther developmental defects, mainly through limiting plastidial energy supply to developing floral tissues (Huang et al., 2023). Accordingly, we observed that HT down-regulated genes involved in anther and pollen development in the parental lines but not in the NILs (Supplemental Figure S8). Our findings thus suggest that the interaction between HT and *PPD-H1* in the development of the photosynthetic apparatus in the spike may contribute to reproductive success.

Taken together, the parental lines with a mutant *ppd-h1* allele were characterized by strong phenotypic and transcriptional plasticity in response to HT. By contrast, the NILs with a functional wild-type *Ppd-H1* allele exhibited very limited transcriptional changes and were not strongly impaired in inflorescence development nor in floret fertility in response to HT. These observations suggest that *Ppd-H1* maintains transcriptional and developmental stability under HT, thus implying the contribution of *Ppd-H1* to environmental canalization in barley. *PPD-H1* alleles have already been implicated in adaptation to stressful environments through accelerating flowering as a stress escape mechanism (Mansour et al., 2014; Shavrukov et al., 2017; Wiegmann et al., 2019; Slafer et al., 2023). We demonstrate that *PPD-H1* does not only control stress escape but also overall stress resistance, even at the early developmental stages. Spring barley genotypes with a mutant *ppd-h1* allele were selected for

cultivation in Northern Europe despite their overall higher stress susceptibility. The slower reproductive development, and thus increased biomass and grain yield, of the spring barely genotypes may outweigh the higher stress susceptibility of these genotypes in more favorable environments. However, climate change and the occurrence of stress events in the early growth seasons in Northern agricultural areas might change the balance of this trade-off.

4 Materials and Methods

4.1 Plant Materials and Growth Conditions

We used the spring barley cultivars Golden Promise (GP) and Scarlett, and the two derived introgression lines GP-fast (GP background) and S42-IL107 (Scarlett background) to study the interaction between *PPD-H1* and HT on shoot growth and inflorescence development. GP and Scarlett carry a mutant *ppd-h1* allele, with a natural mutation causing a Gly-to-Trp amino acid change in the CCT domain of *Ppd-H1* (Turner et al., 2005). GP-fast (Gol et al., 2021) and S42-IL107 (Schmalenbach et al., 2011; Digel et al., 2015) carry the same wild-type *Ppd-H1* allele introgressed from the winter barley Igri and the wild barley accession (*Hordeum vulgare ssp. spontaneum*) ISR42-8, respectively. To investigate whether HT affected auxin homeostasis in the IM, transgenic reporter lines, HvpPIN1a:HvPIN1a-mVENUS and DR5v2-VENUS-H2B in GP background, were used (Kirschner et al., 2018). These lines were crossed with GP-fast and then self-crossed to obtain the lines with homozygous *Ppd-H1* or *ppd-h1* and with homozygous mVENUS or VENUS markers.

For each experiment, plants were sown in ED73 soil (Einheitserde Werkverband e.V.) mixed with 7% sand and 4 g/L Osmocote Exact Hi.End 3-4M (ICL Group Ltd.) in a 96-well growing tray. Sown seeds were stratified for three days at 4°C in the soil for even germination and then transferred to controlled (PAR 300 µM/m^2s, humidity 60%) growth chambers set either at control (CT; 20°C/16°C, day/night) or at high ambient temperature (HT; 28°C/24°C, day/night).

4.2 Phenotyping

To study the impact of HT on shoot growth, inflorescence and floral development, and yield-related traits, plants of GP, GP-fast, Scarlett, and S42-IL107 were germinated and grown under long-day (LD; 16h/8h, day/night) conditions either at CT or at HT, and allowed to grow until full maturity.

4.2.1 Main Shoot Apex Development

To score the development of the main shoot apex (MSA) under CT and HT, five representative plants per genotype and treatment were dissected every three to four days from emergence to post-pollination. The developmental stage of the MSA was scored according to the Waddington scale (Waddington et al., 1983). This scale rates the progression of spikelet initiation and then the development of the most advanced

floral primordium and the pistil of the MSA. The shoot apex transitions from a vegetative to a reproductive developmental phase between W1.5-2.0. At the double-ridge stage (W2.0), spikelet meristem (SM) and leaf primordia are both formed on the shoot apex. Then, only the SM keeps initiating while differentiating to the stamen primordium stage (W3.5). After W3.5, the stem starts to elongate and the SM initiation stops at around the pistil primordium stage (W4.5). Anthesis and pollination occur during W9.5-10.0.

4.2.2 Spikelet and Floral Meristem Initiation

To score the rate of SM and floral meristem (FM) initiation under LD, 16-23 MSAs of GP and GP-fast and 8-17 MSAs of Scarlett and S42-IL107 under CT and HT were dissected at the double-ridge stage (W2.0), the stamen primordium stage (W3.5), the pistil primordium stage (W4.5), and the style primordium stage (W6.0), in the constant LD experiment. SMs were scored as soon as the double-ridge (W2.0) appeared. The number of SMs included those that had differentiated into floral primordia and organs. An FM was scored as soon as the stamen primordium was initiated (W3.5), and the number of FMs included those that had differentiated floral organs or developed into florets.

4.2.3 Shoot Architecture and Yield-Related Traits

Flowering time was scored in days from emergence from the soil until the awns emerged from the flag leaf, called awn tipping (Zadoks et al., 1974). The shoot phenotypes, such as plant height, above-ground dry biomass, and the number of tillers, spikes, and leaves (on the main culm) were measured on 15-20 plants for GP and GP-fast and on 11-15 plants for Scarlett and S42-IL107 in each condition at plant maturity. Plant height was measured from the soil surface to the spike tip. The spike phenotypes, such as the number of florets and grains, were measured on the MSA from the same plant scored for the shoot phenotypes. Floret fertility was determined by the ratio of the grain number to the mature florets number. The length and width of the grain and the thousand-grain weight (TGW) were measured with the seeds from 10 individual plants per genotype and treatment using the MARVIN Seed Analyser (GTA Sensorik).

4.2.4 Leaf Development

The number of emerged leaves on the main culm was recorded every three to four days, and the leaf appearance rate (LAR) was calculated as the time interval between the sequential emergence of leaves on the main culm on 15 plants per

genotype and treatment. The length and width of all leaf blades on the main culm were measured when they were fully elongated, as seen when the auricles of the leaf were widely open. Leaves from 10 individual plants per genotype and treatment were measured. To analyze the cell size of the leaf blade, epidermal imprints were taken of the second fully elongated leaf (L2) from three plants per genotype and treatment. To minimize the positional effect on the cell size, we selected two adaxial positions at 1/3 from the leaf tip and the base and brushed an area length of ca. 2 cm with nail polish. After drying, epidermal imprints were removed carefully with transparent tape and attached to microscope slides. Images of the imprints were captured, and 30 lateral cells (Wenzel et al., 1997) at each position were measured for the cell length. Cell width was calculated by the number of cells within 600 pixels (0.822 pixel/µm) distance using the software Fiji (Schindelin et al., 2012).

4.2.5 Anther Size and Pollen Viability

The length of anthers was measured at W9.0 from the anthers in the central floret located in the middle of the MSA. Anthers of GP and GP-fast were scored from 10 central florets, from five plants per genotype and treatment. Anthers of Scarlett and S42-IL107 were scored from three central florets, from three plants per genotype and treatment. The length of anthers was measured in Fiji (Schindelin et al., 2012). To measure the pollen viability, pollen from the anthers in the central floret located at the middle of MSA was collected at W9.25 from five plants of GP and GP-fast and from three plants of Scarlett and S42-IL107. Anthers were cut into 2-3 pieces on a microscope slide with a sharp scalpel and collected into a 1.5 mL tube with 50 µL of Alexander Staining solution (Peterson et al., 2010). Pollen were released by vortexing for 10 s, then 10 µL of the well-mixed pollen solution was placed onto the microscope slide for imaging. The number of pollen was counted using the ‘Analyze Particles’ function in Fiji (Schindelin et al., 2012).

4.3 Temperature-Photoperiod Co-Shift Experiment

Seeds of GP and GP-fast were sown in a 96-well growing tray, stratified for three days at 4°C in the soil for even germination, and then transferred to LD, at either CT or HT, until the plants reached the spikelet induction stage (W2.0). At W2.0, the plants of each genotype and treatment were transferred from LD to short-day conditions (SD; 10h/14h, day/night) under either HT or CT. We terminated the SD

treatment at 32 days for GP and at 22 days for GP-fast across all temperature treatments and then transferred the plants to the LD and CT conditions.

The rates of SM and FM initiation were scored by dissecting five MSAs per genotype and treatment every 4-8 days after the shift to SD. The number of SMs was counted from the shift day and included those that had differentiated into floral primordia and organs. The FMs were scored as soon as the stamen primordium was initiated (W3.5), and the number of FMs included those that developed into floral organs.

4.4 Microscopy and Image Analysis

To document the development of the MSA and measure the cell length and width in the leaf epidermal imprints, the length of anthers, and count the number of viable and inviable pollens, we used a Nikon DS-Fi2 digital camera attached to a Nikon SMZ18 stereo microscope to capture the images.

To compare the inflorescence meristem (IM) width and height, three MSAs from each genotype and treatment combination were collected from the double-ridge stage (W2.0) until stamen primordium stage (W3.5) every two to four days in GP and GP-fast. To process the MSAs for the 3D reconstruction by confocal microscopic imaging, MSAs were fixed in 2 mL ice-cold 4% paraformaldehyde in 1% phosphate buffered saline (PBS), and vacuum was applied twice for 15 mins on ice. Then, the fixative was replaced with a fresh 2 mL 4% paraformaldehyde, and the MSAs were kept at 4°C overnight. The next day, the MSAs were washed in 1% PBS four times to remove the fixative and then treated with ClearSee solution (Kurihara et al., 2015) for seven days. The treated MSAs were stained with 0.1% SR2200 cell wall stain (SCRI Renaissance 2200) (Musielak et al., 2015) before imaging using a confocal laser scanning microscope (Olympus, FV3000). The stained MSAs were imaged using a 30x silicon immersion objective, excited at 405 nm, and detected between 415 and 476 nm. The IM border was defined by the first cell in the outermost cortex cell layer that doubled in cell length compared to its distal neighbor (Kirschner et al., 2018) using Fiji Software (Schindelin et al., 2012).

The transgenic reporter lines, HvpPIN1a:HvPIN1a-mVENUS and DR5v2:VENUS-H2B in either GP or GP-fast, were collected from CT or HT growth chamber and dissected using a stereo microscope. DAPI was used to stain the cell wall of the MSA of DR5v2:VENUS-H2B and imaged using a confocal laser scanning microscope

(Olympus, FV3000). mVENUS and VENUS fluorescence was excited using a 514 nm laser, and the emission was detected between 530 and 630 nm. DAPI stain was excited using a 405 nm laser, and the emission was detected between 440-473 nm.

4.5 RT-qPCR

To examine the transcriptional changes of *SHORT VEGETATIVE PHASE* (*SVP-LIKE*) family *MADS-BOX* transcription factors, *BM1*, *BM10*, and *VRT2*, and *CEN* (*CENTRORADIALIS*) in the MSAs of GP and GP-fast grown in temperature-photoperiod co-shift experiment, we conducted RT-qPCR on the MSAs collected at 32 days for GP and 22 days for GP-fast after the shift to SD. Three biological replicates were collected, and each replicate contained eight MSAs dissected under a stereo microscope (Zeiss, Stemi 305). Total RNA was extracted from MSA samples using the miRNeasy Plant Mini Kit (Qiagen) following the manufacturer's instructions and digested with DNase I (Qiagen). Total RNA was used for cDNA synthesis, with oligo dT primer and SuperScript II reverse transcriptase (ThermoFisher). Gene expression levels were determined by RT-qPCR using Luna® Universal qPCR Master Mix (New England Biolabs) and gene-specific primer pairs on a LightCycler480 II machine (Roche). Two technical replicates were used for each biological replicate. The quantification was based on the Ct (threshold cycle) values obtained after RT-qPCR. The relative transcript level of the gene of interest was normalized with the housekeeping gene *HvACTIN* using the $2^{-\Delta\Delta Ct}$ method (Livak and Schmittgen, 2001). Error bars represent the standard deviation of the relative expression within three biological replicates. For detailed information on primer pairs of the genes, see Supplemental Data (Table S8).

4.6 Statistical Test and Plotting of the Phenotypic Traits

Phenotypic data and RT-qPCR results were tested for significance using ANOVA test followed by Tukey's HSD test and were plotted in R (v4.0.5) (R Core Team, 2013). The distribution of data points was presented by boxplots using 'ggplot2' R package (84). The box was bound by the lower (Q1) and the upper (Q3) quartiles, and the length of the box represents the interquartile range (IQR). The lower, middle, and upper quartiles were the values under which 25%, 50%, and 75% of data points were found when they were arranged in increasing order. The whiskers of the boxplot were calculated by Q1-1.5*IQR (lower) or Q3+1.5*IQR (upper). The values outside the whiskers were plotted separately as dots and considered as suspected outliers. The

Tukey's HSD test was conducted to compare samples among genotype and treatment groups using the 'Agricolae' R package (de Mendiburu, 2021) for the phenotypic, confocal microscopic, and RT-qPCR data.

4.7 RNA *in situ* Hybridization

To determine the expression patterns of *FLOWERING LOCUS T2* (*FT2*; *BART1_0-p19119*) and *FLOWERING-PROMOTING FACTOR-LIKE* gene (*FPFL*; *BART1_0-p07358*) in the MSA, RNA *in situ* hybridization was conducted using the protocol described in Sang et al., 2020. The MSAs of GP and GP-fast at W3.5 were used to visualize the expression patterns. Two probes of each gene, ca. 200-400 bp in length within coding and 3'UTR regions of the gene were designed to minimize unspecific signals. Antisense and sense probes were synthesized using T7 and T3 RNA Polymerase (Roche) and labeled with Digoxigenin-11-UTP (Roche). Images were captured by a Nikon DS-Fi2 digital camera attached to a Nikon SMZ18 stereo microscope. For detailed information on the primer pairs of the probe, see Supplemental Data (Table S8).

4.8 Whole Transcriptome Sequencing

To detect changes in the global leaf and MSA transcriptomes in response to HT, we harvested the latest fully elongated leaves on the main culm and developing MSAs of GP and GP-fast grown at LD either under CT or HT at four developmental stages, W1.0, W2.0, W3.5, and W6.0 for RNA-sequencing. Each replicate of MSA samples was collected by pooling ca. 30, 20, 15, and 10 MSAs from individual plants at stages W1.0, W2.0, W3.5, and W6.0, respectively, and a total of four biological replicates for each genotype, treatment, and developmental stage combination. All MSA samples were collected under a stereo microscope in the environment where the plant grew. For leaf samples, each replicate contained the middle section of the latest fully elongated leaf on the main culm pooled from three individual plants. A total of three to four biological replicates of MSA and leaf samples were used across genotype, treatment, and developmental stage.

Total RNA was extracted from MSA and leaf samples using the RNeasy Plant Mini Kit (Qiagen) with beta-mercaptoethanol added following the manufacturer's instructions and digested with DNase I (Qiagen). RNA samples passing a cutoff of RNA Integrity Number (RIN) $\geq$ 6 were used for mRNA library preparation with poly A enrichment.

Paired-end 150 bp sequencing was performed on NovaSeq 6000 sequencing platform, and at least 5G of clean reads data per sample were generated by Novogene Co., Ltd, UK. Q30 of each sample was ranged from 92% to 94%. All samples passed the assessment of the adaptor and GC contents by FastQC (Andrews, 2010) (Table S7). For detailed information on quality reports of the reads generated by MultiQC (Ewels et al., 2016), see Supplemental Data (Table S7).

4.9 RNAseq Analyses

To quantify transcripts, all clean reads were mapped to the BaRT1 (Rapazote-Flores et al., 2019) reference using Salmon (v. 0.14.1) (Patro et al., 2017), and the mapping rates were estimated with an average of ~93%. For detailed information on mapping rate results, see Supplemental Data (Table S7). We kept transcripts with a minimum of 1 CPM (counts per million) in at least three samples of leaves or MSAs at W1.0-3.5 and W6.0, respectively. To improve the annotation of the reference, we aligned the CDS sequences of BaRT1 with BLASTX (v2.12.0) against the peptide sequences of *Arabidopsis thaliana* TAIR10, with pident of 25 and e-value of 10^{-6}. A reciprocal BLASTN (v2.13.0) alignment was conducted between BaRT1 and barley MorexV3 (Mascher et al., 2021) using CDS sequences, and the best hit was identified when there was a reciprocal best hit between a gene model in both directions.

Analyses of leaf samples were conducted on 24541 expressed genes. For the MSA samples, analyses were conducted on 24316 genes expressed among the early developmental stage (W1.0-W3.5) and on 27077 genes expressed at W6.0. Principle component analysis (PCA) and normalization of TPM (transcript per million) were conducted using ‘ThreeDRNAseq’ R package (v2.0.1) (Guo et al., 2021).

4.9.1 Identification of Temperature-Responsive Differentially Expressed Genes in Leaves

To identify differentially expressed genes (DEGs) in response to HT in leaf samples of GP and GP-fast, a three-way ANOVA was calculated with TPM using the ANOVA function ‘aov’ in R, with the script of aov(TPM ~ genotype*treatment*developmental stage, data=[data source]). The *p*-value of the temperature effect (ANOVA.*p.temperature*) of each gene was adjusted by the Benjamini-Hochberg (BH) procedure. A threshold of ANOVA.*p.temperature*<0.01 was applied to determine statistical significance. All genes significantly different between temperatures in the ANOVA test were then subjected to pairwise comparisons for

detecting significant transcriptional changes between HT and CT conditions within each genotype and developmental stage, using the count-based Fisher's Exact Test in R package 'EdgeR' (v3.32.1) (Robinson et al., 2010). The FDR of each gene was adjusted by the BH procedure (BH.FDR), thus the gene with BH.FDR < 0.01 and $|\log_2 FC| \geq 1$ or in at least three stages of GP and GP-fast was referred to as a thermal-responsive gene.

To confirm the thermoresponsiveness of the gene detected in GP and GP-fast, we tested the transcriptional changes of the gene in Scarlett and S42-IL107 at W3.5 and W6.0, respectively. The pairwise comparisons between CT and HT by the count-based Fisher's Exact Test were conducted in Scarlett and S42-IL107 at W3.5 and W6.0. Genes with BH.FDR<0.01 and $|\log_2 FC| > 0$ either W3.5 or W6.0 in Scarlett and S42-IL107 were considered as thermal responsive DEGs. To reduce the interference from the genes other than *PPD-H1* within the introgression regions, we focused on genes exhibiting up- or down-regulation in response to HT in both GP and Scarlett or in both GP-fast and S42-IL107. For detailed information on statistics and results, see Supplemental Data (Table S3).

4.9.2 Identification of Temperature-Responsive Differentially Expressed Genes in Main Shoot Apices

As the MSA at W6.0 already contains florets with many developed floral organs, like anthers, awns, and pistil primordia, the transcriptome of MSA at W6.0 strongly differed from that of the MSAs at early developmental stages (W1.0-W3.5). For this reason, we analyzed the RNA-seq data from MSAs at W6.0 separately.

To identify DEGs in response to HT in MSA samples of GP and GP-fast at early developmental stage (W1.0-W3.5), a three-way ANOVA followed by the count-based Fisher's Exact Test was conducted in MSA samples, as described above in the leaf samples of GP and GP-fast. Genes with significant regulation as revealed by ANOVA.*p.temperature*<0.01 and $|\log_2 FC| \geq 1$ with BH.FDR <0.01 in at least one stage among W1.0-3.5 was considered as HT-dependent DEG in the MSA at the early developmental stage. In the MSA at W6.0, DEGs in response to HT were identified by pairwise comparisons between CT and HT within each genotype using the Fisher's Exact test. For detailed information on statistics and results, see Supplemental Data (Table S6).

To confirm the thermoresponsiveness of the genes detected in GP and GP-fast, we tested the significance of the transcriptional differences of the gene in the MSA of Scarlett and S42-IL107 at W3.5 and W6.0, respectively, using the count-based Fisher's Exact Test as described above in leaf samples of Scarlett and S42-IL107. Genes with a significant regulation at BH.FDR < 0.01 and $|\log_2 FC| > 0$ at either W3.5 or W6.0 were considered as thermal responsive DEGs in Scarlett and S42-IL107. To reduce the interference from the genes other than *PPD-H1* within the introgression regions, we focused on genes exhibiting up- or down-regulation in response to HT in both GP and Scarlett or GP-fast and S42-IL107. For detailed information on statistics and results, see Supplemental Data (Table S6).

4.9.3 Identification of *PPD-H1*-Dependent Differentially Expressed Genes in Leaves and Main Shoot Apices

To identify *PPD-H1*-dependent DEGs between the GP and GP-fast in the leaf, we applied pairwise comparisons between GP and GP-fast at each developmental stage, using the count-based Fisher's Exact test under CT and HT, respectively. Genes significantly regulated between GP and GP-fast with BH.FDR < 0.01 and $|\log_2 FC| \geq 1$ in at least three developmental stages were considered as *PPD-H1*-dependent DEGs in the leaf. *PPD-H1*-dependent DEGs detected in GP and GP-fast were then tested in Scarlett and S42-IL107 at W3.5 and W6.0, respectively, using the count-based Fisher's Exact test, as described above for the HT-dependent DEGs in the leaf. We focused on genes exhibiting up- or down-regulation by *PPD-H1* between GP and GP-fast and between Scarlett and S42-IL107.

As for the MSA, *PPD-H1*-dependent DEGs between GP and GP-fast were detected using the count-based Fisher's Exact test under CT and HT, respectively. Genes with BH.FDR < 0.01 and $|\log_2 FC| \geq 1$ in at least one developmental stage were considered as *PPD-H1*-dependent DEGs in the MSA. The *PPD-H1*-dependent DEG detected in GP and GP-fast was then tested in Scarlett and S42-IL107 at W3.5 and W6.0, respectively, using the count-based Fisher's Exact test, as described above for the HT-dependent DEGs in the MSA. We focused on genes exhibiting up- or down-regulation by *PPD-H1* between GP and GP-fast and between Scarlett and S42-IL107. For detailed information on statistics and results, see Supplemental Data (Table S4).

4.9.4 Identification of Genes Associated with Developmental Stage in Main Shoot Apices at the Early Developmental Stage

Since HT impaired MSA development, we only used the MSA samples collected under CT of GP and GP-fast at W1.0, W2.0, and W3.5 for a two-way ANOVA calculated by the TPM with the script of aov(TPM ~ genotype*developmental stage, data=[data source]). The *p*-value of the developmental stage effect (ANOVA.*p.development*) of each gene was adjusted by the BH procedure. A threshold of ANOVA.*p.developmen* < 0.01 was applied to determine statistical significance. All significant genes in the ANOVA were then subjected to pairwise comparisons between developmental stages within each genotype, using Fisher's Exact Test with BH.FDR <0.01 and $|\log_2 FC| \geq 1$ detected at any of the pairwise comparisons and genotypes were referred to as development-regulated DEGs. For detailed information on statistics and results, see Supplemental Data (Table S6).

4.9.5 Gene Ontology Enrichment Analyses and Plotting

To identify significantly enriched gene ontology (GO) terms, we conducted GO enrichment analysis using 'GOEnrichment' tool of *Triticeae Gene Tribe* database (Chen et al., 2020) with BH.*p*-value < 0.05 (Table S4, S5). Heatmaps for GO enrichment were generated with the $-\log_{10}$(FDR) values of the top ten biological function GO terms by 'ThreeDRNAseq' R package(Guo et al., 2021). For the complete information on all GO terms and genes for each GO term, see Supplemental Data (Table S4, S5). Heatmaps of gene expression in selected GO terms were generated with the $\log_{10}$(TPM+1) values by 'ThreeDRNAseq' R package (Guo et al., 2021). The distance matrix was computed using the Euclidean method.

5 Figures

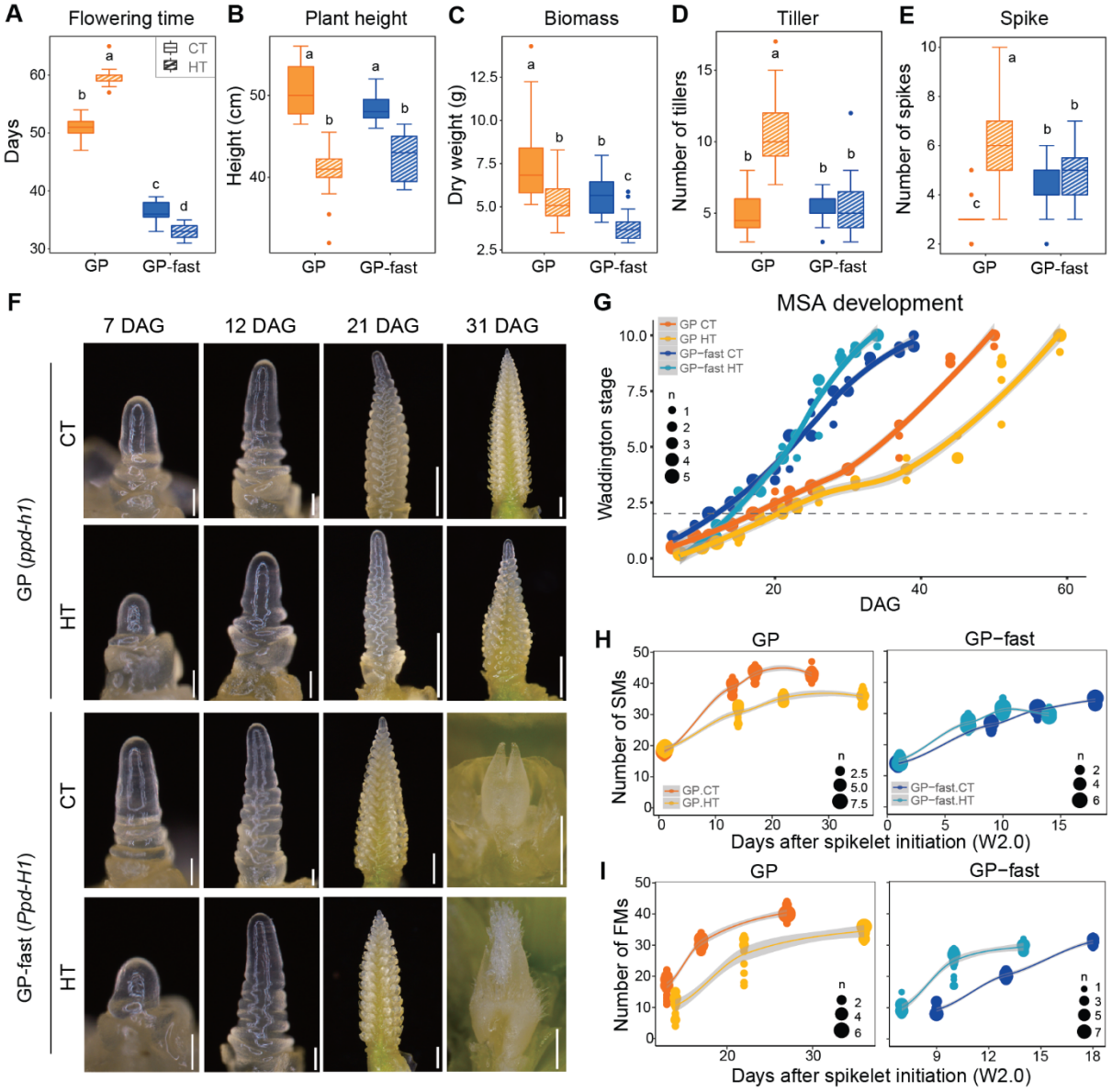

Figure 1. Effects of High Ambient Temperature on Shoot Growth and Spike Development in Golden Promise and GP-Fast

Shoot architecture and main shoot apex (MSA) development of spring barley cultivar Golden Promise (GP, *ppd-h1* allele) and its derived near-isogenic line GP-fast (*Ppd-H1* allele) under long-day (16h/8h, day/night) control (CT; 20°C/16°C, day/night) and high ambient temperatures (HT; 28°C/24°C, day/night). (A) Flowering time in days from emergence until the appearance of the first awn from the flag leaf. (B) Plant height, (C) above-ground dry biomass, and (D-E) number of tillers and spikes were scored at full maturity (n = 15-20). (F-G) Development of the MSA of GP and GP-fast after germination under CT and HT, stages according to Waddington et al. (1983). Scale bar = 100 µm (for 7 and 12 days); Scale bar = 500 µm (for 21 and 31 days). DAG indicates days after germination. The gray dashed line marks the transition (W2.0) from vegetative to reproductive MSA. (H-I) Comparison of the number of spikelet meristems (SMs) at W2.0, W3.5, W4.5, and W6.0, and the number of floral meristems (FMs)

at W3.5, W4.5, and W6.0 in GP and GP-fast under CT and HT (n = 10-20). Box plots show the median and interquartile range. Whisker lines of box plots show the range of minimum and maximum values. Statistical groups are assigned using ANOVA followed by Tukey's HSD test. Different letters indicate statistically significant differences between groups (p<0.05). Dot sizes indicate the number of overlapping samples. Trend lines are calculated using a polynomial regression (Loess smooth line). Gray areas show the 95% confidence interval.

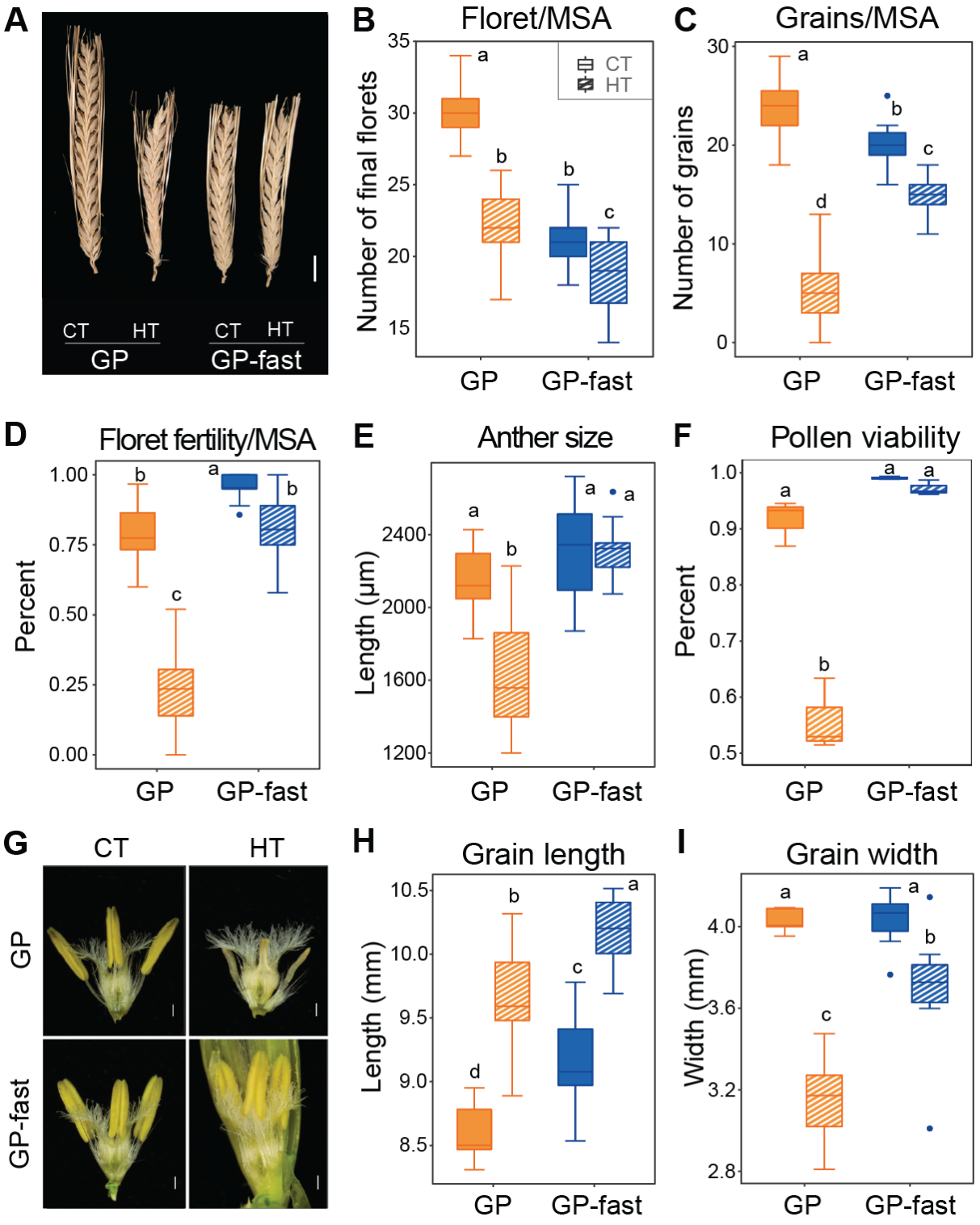

Figure 2. Effects of High Ambient Temperature on Fertility and Grain Set in Golden Promise and GP-fast

Yield-related traits of spring barley cultivar Golden Promise (GP, *ppd-h1* allele) and its derived near-isogenic line GP-fast (*Ppd-H1* allele) under long-day (16h/8h, day/night) control (CT; 20°C/16°C, day/night) and high ambient temperatures (HT; 28°C/24°C, day/night). (A) Main spike morphology of GP and GP-fast under CT and HT. Scale bar = 1 cm. (B-D) Comparison of floret and grain number, and floret fertility, on the main shoot apex (MSA) across genotype and treatment. Floret fertility was

determined by the ratio of the grain number to the mature floret number. (E-F) Comparison of anther length and pollen viability from central florets at the middle of MSA across genotype and treatment at W9.5. For the anther length, anthers from 10 central florets, collected from five plants per genotype and treatment were scored; for the pollen viability, pollens from central florets at the middle of the MSA of five plants per genotype and treatment were scored. (G) Morphology of pistils and anthers in the florets from the central floret at the middle of MSA of GP and GP-fast under CT and HT around W9.5-10.0. Scale bar = 100 μm. (H-I) Comparison of grain length and width across genotype and treatment (n = 10). Box plots show the median and interquartile range. Whisker lines of box plots show the range of minimum and maximum values. Statistical groups are assigned using ANOVA followed by Tukey's HSD test. Different letters indicate statistically significant differences between groups (p<0.05).

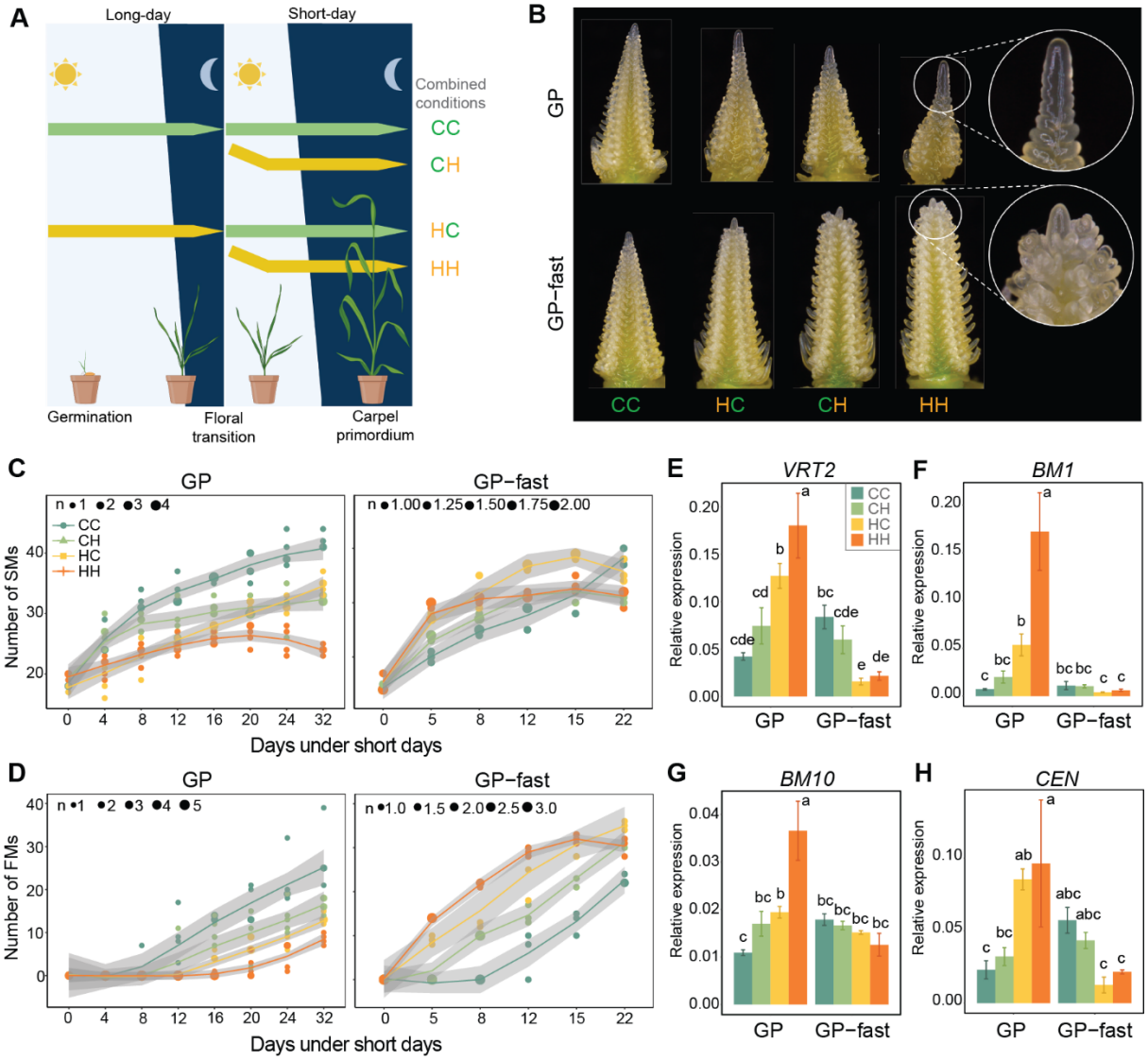

Figure 3. High Ambient Temperature Treatment before and after Spikelet Initiation Affects Spikelet Meristem and Floral Meristem Induction in a Genotype-Dependent Manner

(A) Schematic representation of the experimental setup of the temperature-photoperiod co-shift experiment. Spring barley cultivar Golden Promise (GP, *ppd-h1* allele) and its derived near-isogenic line GP-fast (*Ppd-H1* allele) were germinated and grown at long-day (LD; 16h/8h, day/night) either under control (CT; 20°C/16°C, day/night) or high ambient temperature (HT; 28°C/24°C, day/night) until the spikelet induction stage (W2.0), then shifted to short-day (SD; 10h/14h, light/dark) at either CT or HT to monitor the main shoot apex (MSA) development. Plants were transferred from LD and CT to SD under either CT (CC) or HT (CH). Likewise, plants were transferred from LD and HT to SD under either CT (HC) or HT (HH). (B) Representative MSAs of GP and GP-fast after the shift, at 32 and 22 days, respectively. (C-D) Comparison of the number of spikelet meristems (SMs) and floral meristems (FMs) in GP and GP-fast under four conditions after the shift to SD (n = 5). (E-H) Comparison of the transcript levels of floral repressors, *SHORT VEGETATIVE PHASE-LIKE* (*SVP-LIKE*) family genes, *VRT2*, *BM1*, *BM10*, and *CENTRORADIALIS* (*CEN*) in MSAs of GP at 32 days after the shift to SD and at 22 days after the shift to SD in GP-fast by RT-qPCR (n = 3, 5-8 MSAs pooled per replicate). The stages of the

MSAs collected were around stamen primordium (W3.5) to pistil primordium (W4.5) stage, as indicated in (B). The relative expression of the gene was normalized with the expression of *HvACTIN*. Error bars show the standard deviation. Statistical groups were assigned using ANOVA followed by Tukey's HSD test. Different letters indicate statistically significant differences between groups ($p<0.05$). Dot sizes indicate the number of overlapping samples. Trend lines are calculated using a polynomial regression (Loess smooth line). Gray areas show the 95% confidence interval.

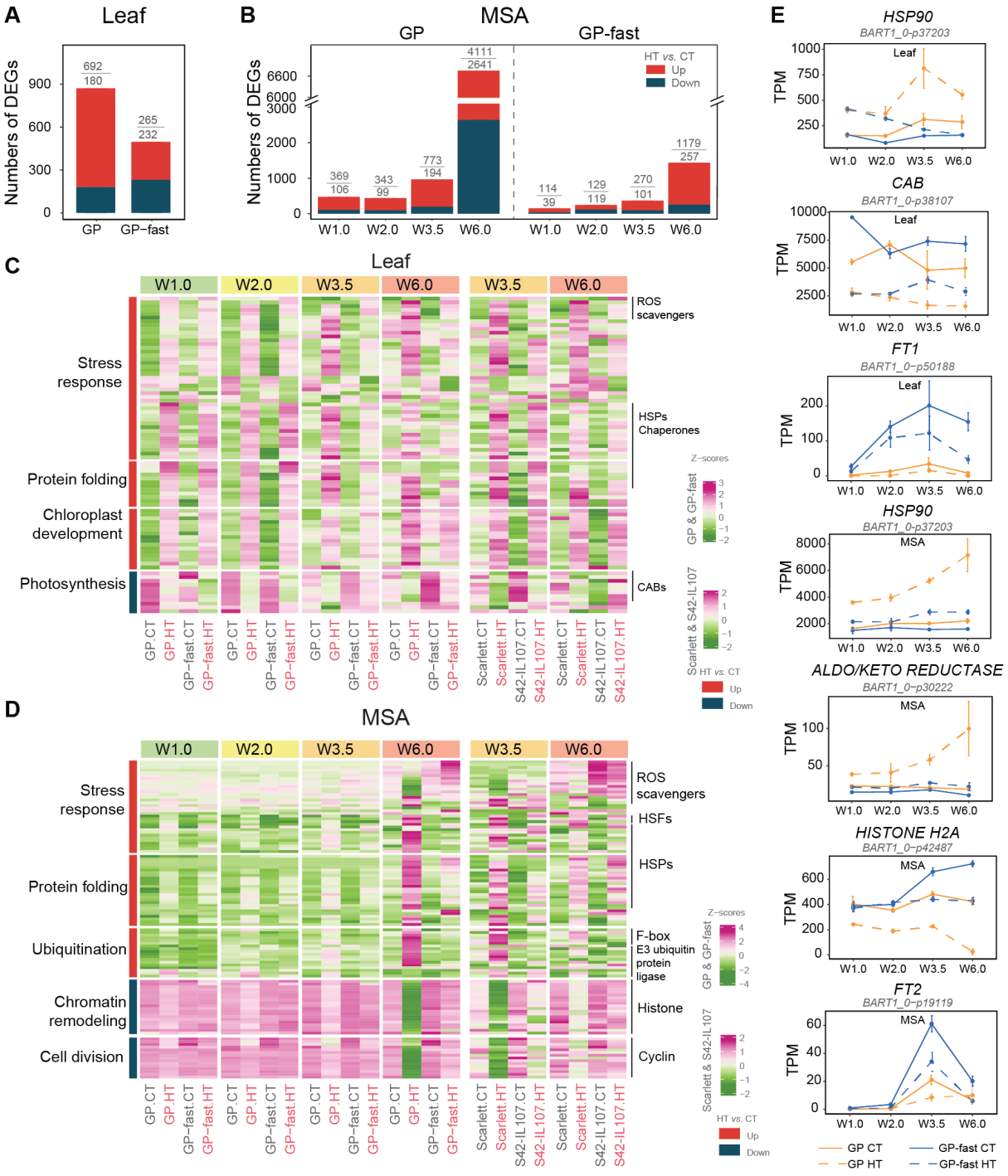

Figure 4. Thermal-Transcriptome Reprogramming in the Leaf and Main Shoot Apex

(A-B) Total number of differentially expressed genes (DEGs) in leaf and main shoot apex (MSA) between control (CT; 20°C/16°C, day/night) and high ambient temperature (HT; 28°C/24°C, day/night) under long-day (16h/8h, day/night) in spring barley cultivar Golden Promise (GP, *ppd-h1* allele) and its derived near-isogenic line GP-fast (*Ppd-H1* allele). Red bars represent up-regulated DEGs (BH.FDR < 0.01, $\log_2$FC ≥ 1 and dark blue bars represent down-regulated DEGs (BH.FDR < 0.01, $\log_2$FC ≤ -1). For details, see the Methods and Supplemental Data. (C-D) Heatmaps of DEGs from significant gene ontology enriched terms in leaf and in MSA. The color scale represents the Z-score values of transcripts

per million (TPM). (E) Expression of representative DEGs in leaf and MSA. Expression values are represented by TPM in GP (orange) and GP-fast (blue) under CT (solid line) and HT (dashed line). Error bars indicate standard deviation within biological replicates. *HSP90*, *HEAT SHOCK PROTEIN 90; CAB*, *CHLOROPHYLL A-B BINDING PROTEIN* gene; *FT1*, *FLOWERING LOCUS T1*; *FT2*, *FLOWERING LOCUS T2*.

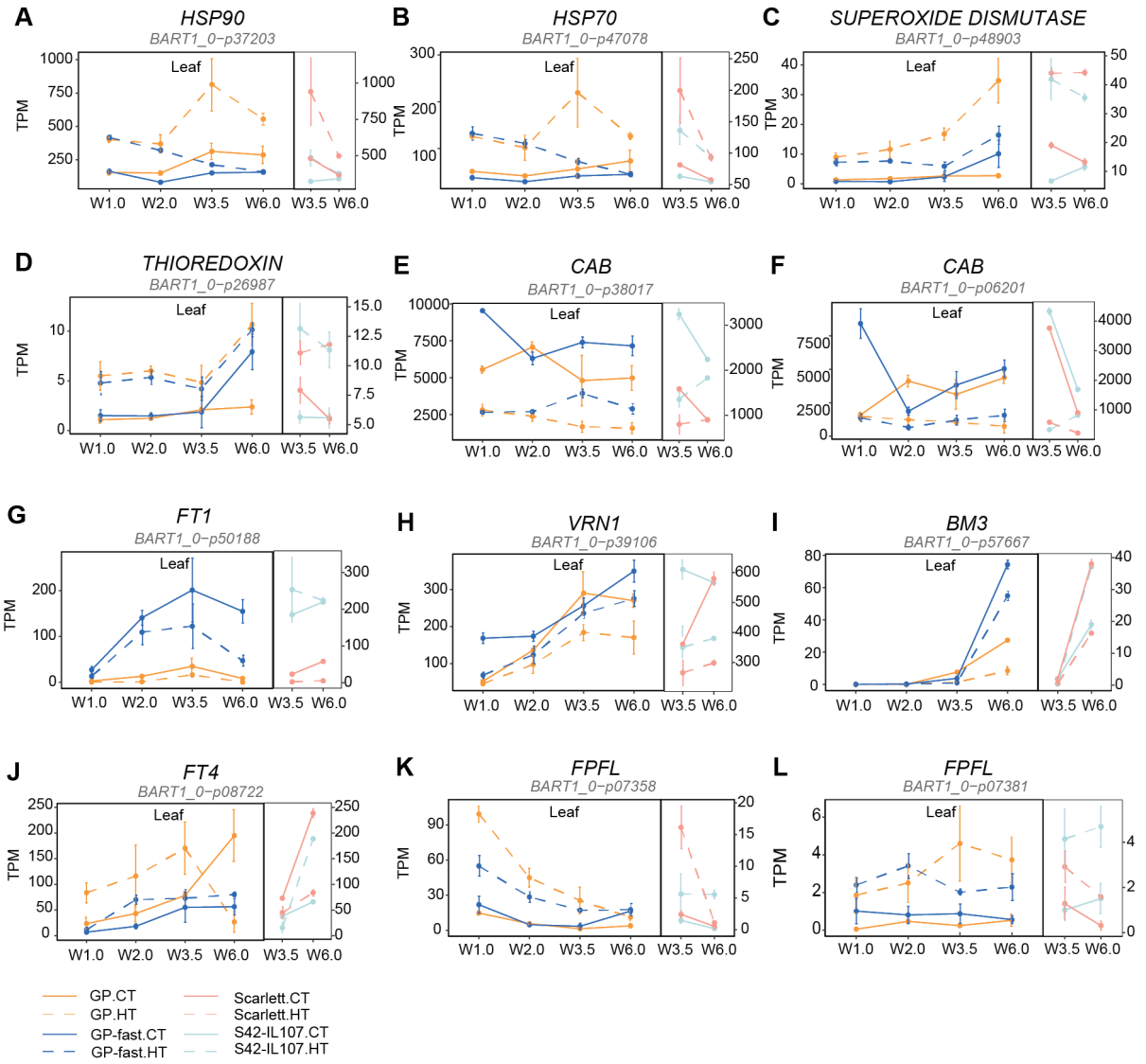

Figure 5. Expression of Representative Thermal-Responsive Genes in the Leaf

Transcript levels of genes involved in heat response (A-B) and redox homeostasis (C-D) that were up-regulated in response to high ambient temperature (HT; 28°C /24°C, day/night), whereas the genes involved in photosynthesis (E-F) were down-regulated in response to HT in spring barley cultivars Golden Promise (GP, *ppd-h1* allele) and Scarlett (*ppd-h1* allele), and the near-isogenic lines, GP-fast (*Ppd-H1* allele) and S42-IL107 (*Ppd-H1* allele). Transcript levels of genes acting as flowering promoters (G-I) were down-regulated in response to HT. Transcript levels of genes acting as repressors (J-L) were up-regulated in response to HT. Gene expression was reported in transcripts per million (TPM) of GP (orange), GP-fast (blue), Scarlett (light blue), and S42-IL107 (pink) under long-day (LD; 16h/8h, day/night) control ambient temperature (CT; 20°C/16°C, day/night; solid line) and HT (dashed line). Error bars indicate the standard deviation of biological replicates (n = 3-4). *HSP90*, *HEAT SHOCK PROTEIN 90; HSP70*, *HEAT SHOCK PROTEIN 70; ARC5*, *ACCUMULATION AND REPLICATION OF CHLOROPLAST 5*; *CAB*, *CHLOROPHYLL A-B BINDING PROTEIN* gene; *FT1*, *FLOWERING LOCUS T1*; *VRN1*, *VERNALIZATION 1*; *BM3*, *BARLEY MADS-BOX 3*; *FT4*, *FLOWERING LOCUS T4*; *FPFL*, *FLOWERING PROMOTING FACTOR-LIKE* gene.

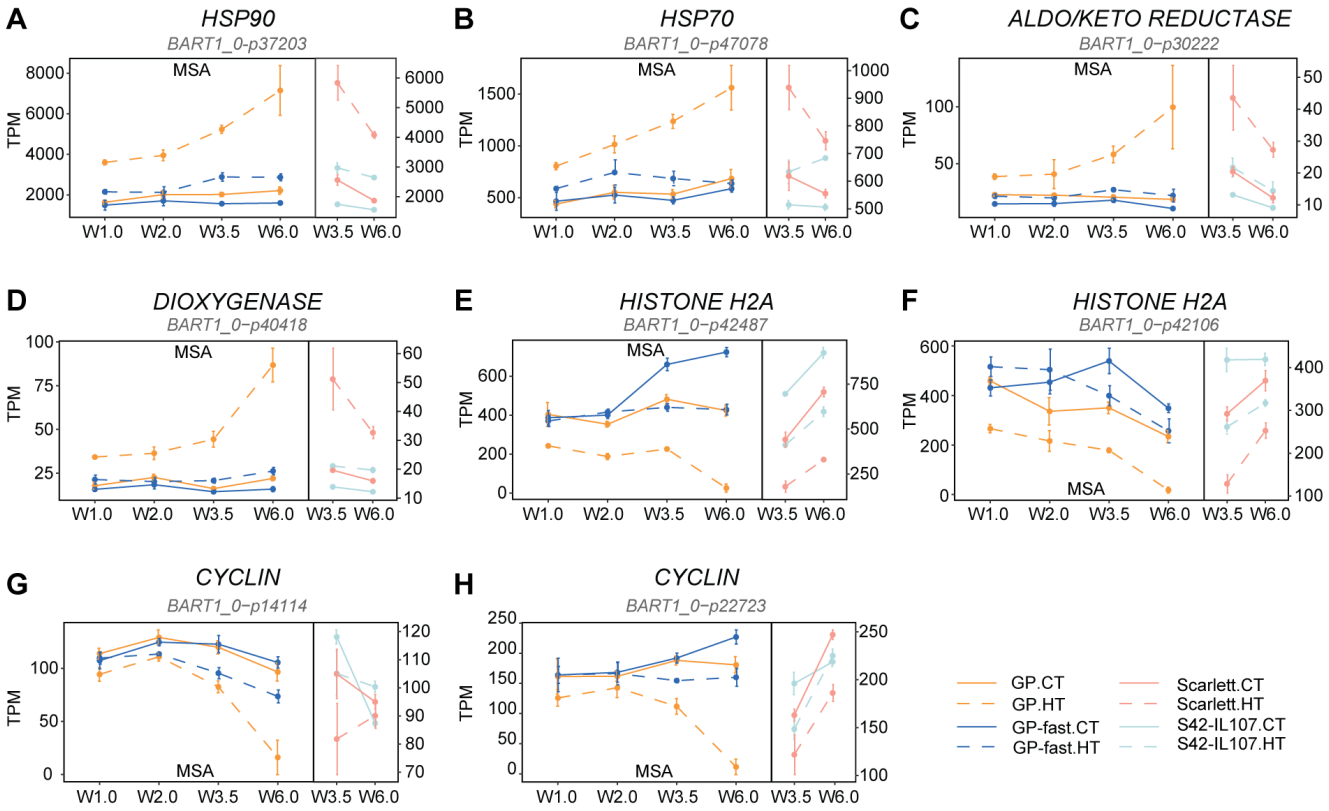

Figure 6: Expression of Representative Thermal-Responsive Genes in Main Shoot Apex

Transcript levels of genes involved in heat response (A-B) and redox homeostasis (C-D) pathways were more strongly up-regulated in response to high ambient temperature (HT; 28°C/24°C, day/night) in the spring barley Golden Promise (GP, *ppd-h1* allele) and Scarlett (*ppd-h1* allele) than in their respective near-isogenic lines, GP-fast (*Ppd-H1* allele) and S42-IL107 (*Ppd-H1* allele). By contrast, genes involved in chromatin remodeling (E-F) and cell cycle (G-H) pathways were more strongly down-regulated in response to HT in GP and Scarlett than in GP-fast and S42-IL107. Gene expression was reported in transcripts per million (TPM) of GP (orange), GP-fast (blue), Scarlett (light blue), and S42-IL107 (pink) under long-day (LD; 16h/8h, day/night) and control ambient temperature (CT; 20 °C/16°C, day/night; solid line) and HT (dashed line). Error bars indicate the standard deviation among biological replicates (n = 4). *HSP90*, *HEAT SHOCK PROTEIN 90; HSP70*, *HEAT SHOCK PROTEIN 70*.

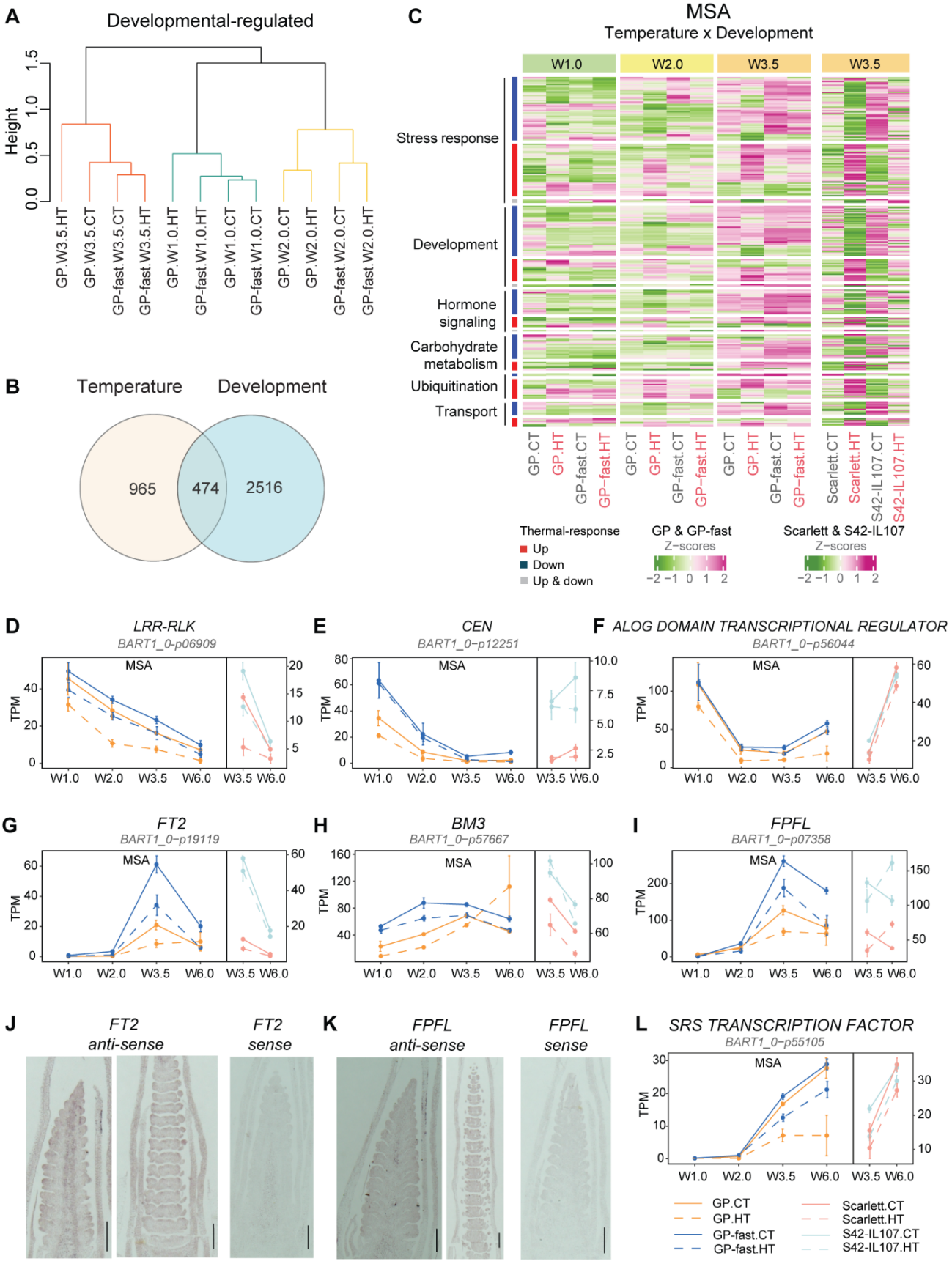
A
Developmental-regulated
Height
0.0
0.5
1.0
1.5
GP.W3.5.HT
GP.W3.5.CT
GP-fast.W3.5.CT
GP-fast.W3.5.HT
GP.W1.0.HT
GP-fast.W1.0.HT
GP.W1.0.CT
GP-fast.W1.0.CT
GP.W2.0.CT
GP.W2.0.HT
GP-fast.W2.0.CT
GP-fast.W2.0.HT
B
Temperature
Development
965
474
2516
C
MSA
Temperature x Development
W1.0
W2.0
W3.5
W3.5
Stress response
Development
Hormone signaling
Carbohydrate metabolism
Ubiquitination
Transport
GP.CT
GP.HT
GP-fast.CT
GP-fast.HT
Scarlett.CT
Scarlett.HT
S42-IL107.CT
S42-IL107.HT
Thermal-response
Up
Down
Up & down
GP & GP-fast
Z-scores
Scarlett & S42-IL107
Z-scores
D
LRR-RLK
BART1_0-p06909
E
CEN
BART1_0-p12251
F
ALOG DOMAIN TRANSCRIPTIONAL REGULATOR
BART1_0-p56044
G
FT2
BART1_0-p19119
H
BM3
BART1_0-p57667
I
FPFL
BART1_0-p07358
MSA
TPM
W1.0
W2.0
W3.5
W6.0
J
FT2
anti-sense
FT2
sense
K
FPFL
anti-sense
FPFL
sense
L
SRS TRANSCRIPTION FACTOR
BART1_0-p55105
GP.CT
GP.HT
GP-fast.CT
GP-fast.HT
Scarlett.CT
Scarlett.HT
S42-IL107.CT
S42-IL107.HT

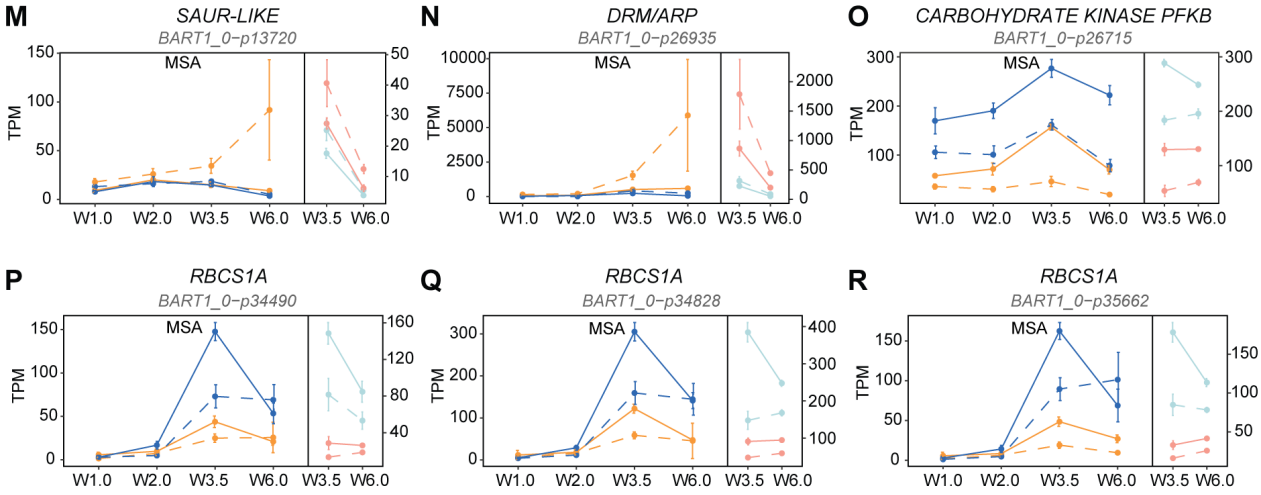

Figure 7. Effects of High Ambient Temperature on the Expression of Developmental Genes in the Main Shoot Apex

(A) Unsupervised hierarchical cluster analysis of development-regulated genes in the main shoot apex (MSA) of spring barley Golden Promise (GP, *ppd-h1* allele) and its derived near-isogenic line GP-fast (*Ppd-H1* allele) during the early developmental stage (W1.0-W3.5). (B) Venn diagram of genes that were regulated by development and temperature in the MSA. (C) The heatmap represents the expression of genes co-regulated by temperature and development in the MSA, which primarily function in stress response, development, hormone signaling, carbohydrate metabolism, ubiquitination, and transmembrane transport regulatory pathways. The color scale represents the Z-score values of transcripts per million (TPM). (D-I) RNA-sequencing derived expression data of stem cell maintenance genes (D-F) and floral homeotic genes (G-I). (J-K) RNA *in situ* hybridization using *FT2* (*BART1_0-p19119*) and *FPFL* (*BART1_0-p07358*) as probes on longitudinal sections through the MSA of GP-fast at stamen primordium stage (W3.5). Scale bar = 500 µm. Thermal-responsive genes related to auxin biosynthesis and signaling (L-N) and carbon metabolism (O-R) are shown. Gene expression was reported in transcripts per million (TPM) of GP (orange), GP-fast (blue), Scarlett (light blue), and S42-IL107 (pink) under long-day (16h/8h, day/night) control ambient temperature (CT; 20°C/16°C, day/night; solid line) and high ambient temperature (HT; 28°C/24°C, dashed line). Error bars indicate the standard deviation of biological replicates (n = 3-4). *LRR-RLK, LEUCINE-RICH REPEAT RECEPTOR-LIKE PROTEIN KINASE*; *CEN*, *CENTRORADIALIS*; *FT2*, *FLOWERING LOCUS T2*; *BM3*, *BARLEY MADS-BOX 3*; *FPFL*, *FLOWERING PROMOTING FACTOR-LIKE* gene; *DRM/ARP*, *DORMANCY/AUXIN ASSOCIATED FAMILY* gene; *RBCS1A*, *RIBULOSE BISPHOSPHATE CARBOXYLASE SMALL CHAIN 1A*.

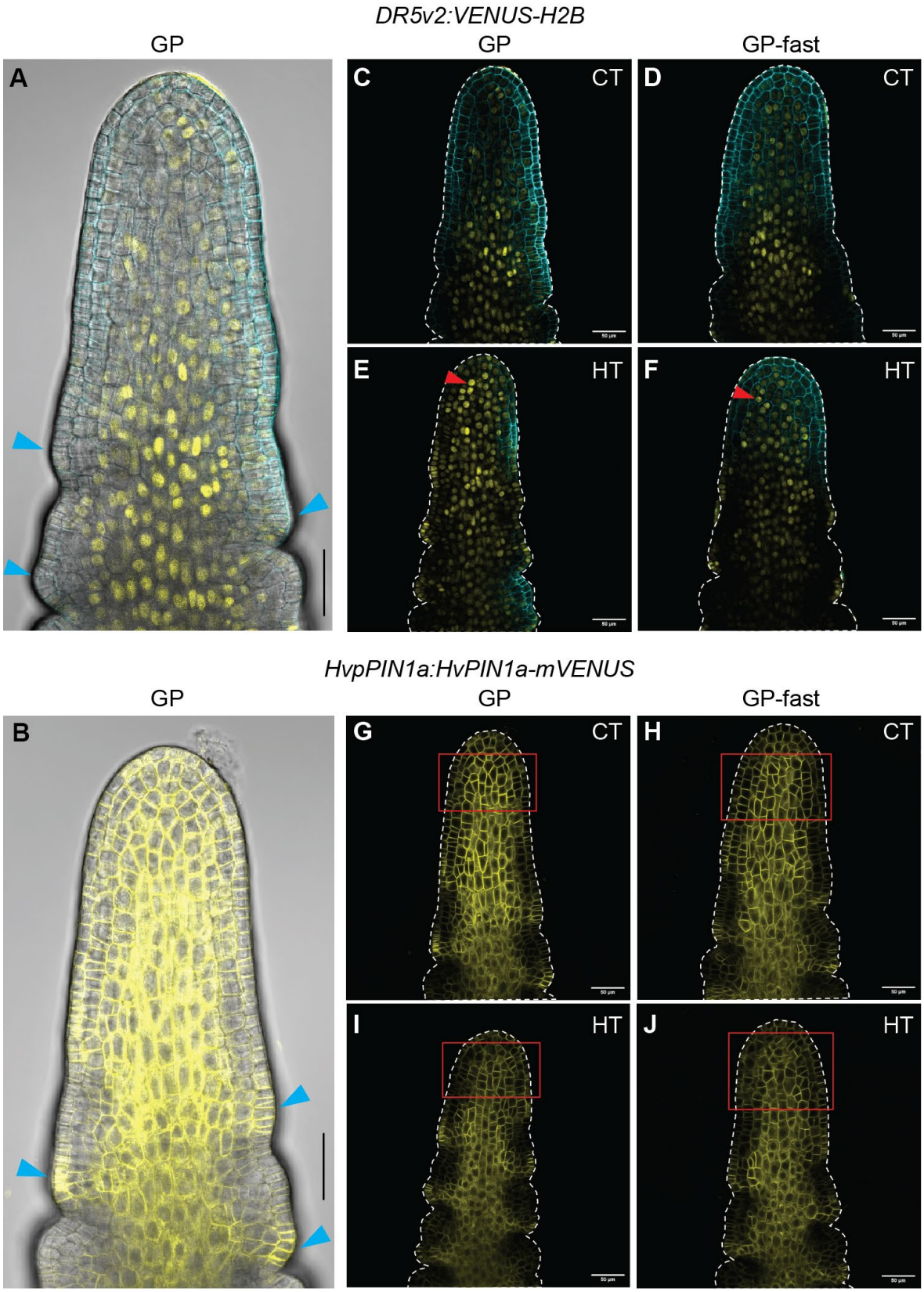

Figure 8. High Ambient Temperature Affects Auxin Polar Transport and Local Concentration In the Inflorescence Meristem

(A-B) Representative images of *DR5v2:VENUS-H2B* and *HvpPIN1a:HvPIN1a-mVENUS* expression in the inflorescence meristem (IM) of Golden Promise (GP, *ppd-h1* allele) at spikelet induction stage (W2.0) under long-day (LD, 16h/8h, day/night) under control (CT; 20°C/16°C, day/night). (C-D) Representative images of *DR5v2:VENUS-H2B* expression in the IM of GP and GP-derived near-isogenic line GP-fast (*Ppd-H1* allele) at W2.0 under CT. (n > 20). (E-F) Representative images of *DR5v2:VENUS-H2B* expression in the IM of GP and GP-fast at W2.0 under high ambient temperature (HT; 28°C/24°C, day/night) conditions. (n > 20). (G-H) Representative images of *DR5v2:VENUS-H2B* expression in the IM of GP and GP-fast at W2.0 under CT. (n > 20). (I-J) Representative images of *HvpPIN1a:HvPIN1a-mVENUS* in the IM of GP and GP-fast at W2.0 under HT. (n > 20). The images were obtained with transmitted light and mVENUS emission: The red frames indicate the region where the expression of *HvpPIN1a:HvPIN1a-mVENUS* differed between CT and HT. The red triangles indicate the region where the *DR5v2:VENUS-H2B* was induced under HT. The blue triangles indicate the leaf primordia. Scale bar = 60 µm.

6 Supplemental Data

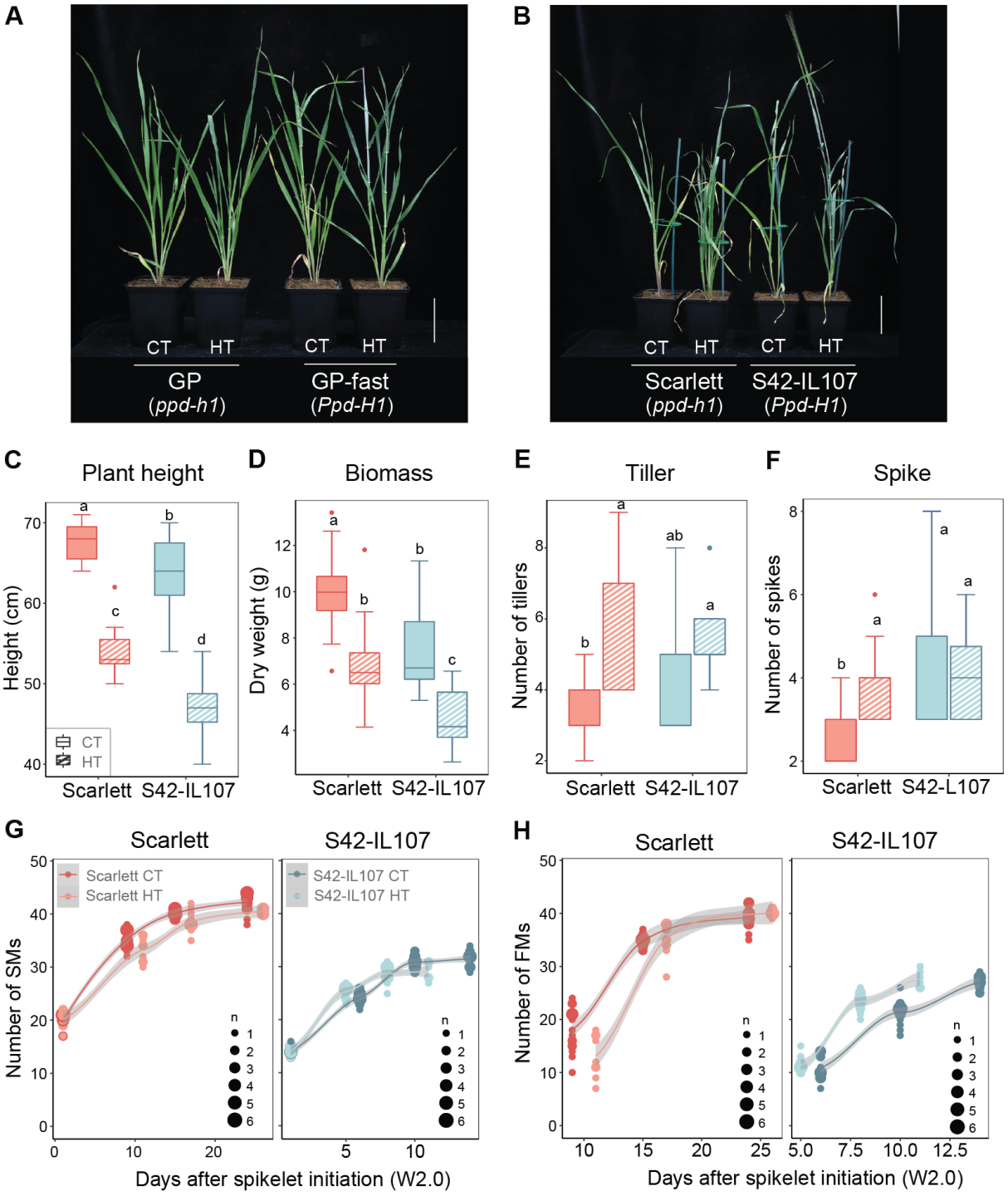

Figure S1. Effects of High Ambient Temperature on Shoot Growth and Spike Development in Scarlett and S42-IL107

(A-B) Plant morphology of spring barley cultivar Golden Promise (GP, *ppd-h1* allele) and Scarlett (*ppd-h1* allele) and their derived near-isogenic lines GP-fast (*Ppd-H1* allele) and S42-IL107 (*Ppd-H1* allele) under long-day (16h/8h, day/night) control (CT; 20°C/16°C, day/night) and high ambient temperatures (HT; 28°C/24°C, day/night). (C) Plant height, (D) above-ground dry biomass, and (E-F) number of tillers

and spikes of Scarlett and S42-IL107 were scored at full maturity (n = 11-15). (G-H) Comparison of the number of spikelet meristems (SMs) at W2.0, W3.5, W4.5, and W6.0 and the number of floral meristems (FMs) at W3.5, W4.5, and W6.0 in Scarlett and S42-IL107 under CT and HT (n = 6-17). Box plots show the median and interquartile range. Whisker lines of box plots show the range of the minimum and maximum values. Statistical groups were assigned using Tukey's HSD test. Different letters indicate statistically significant differences between groups ($p < 0.05$). Dot sizes indicate the number of overlapping samples. Trend lines are calculated using a polynomial regression (Loess smooth line). Gray areas show the 95% confidence interval.

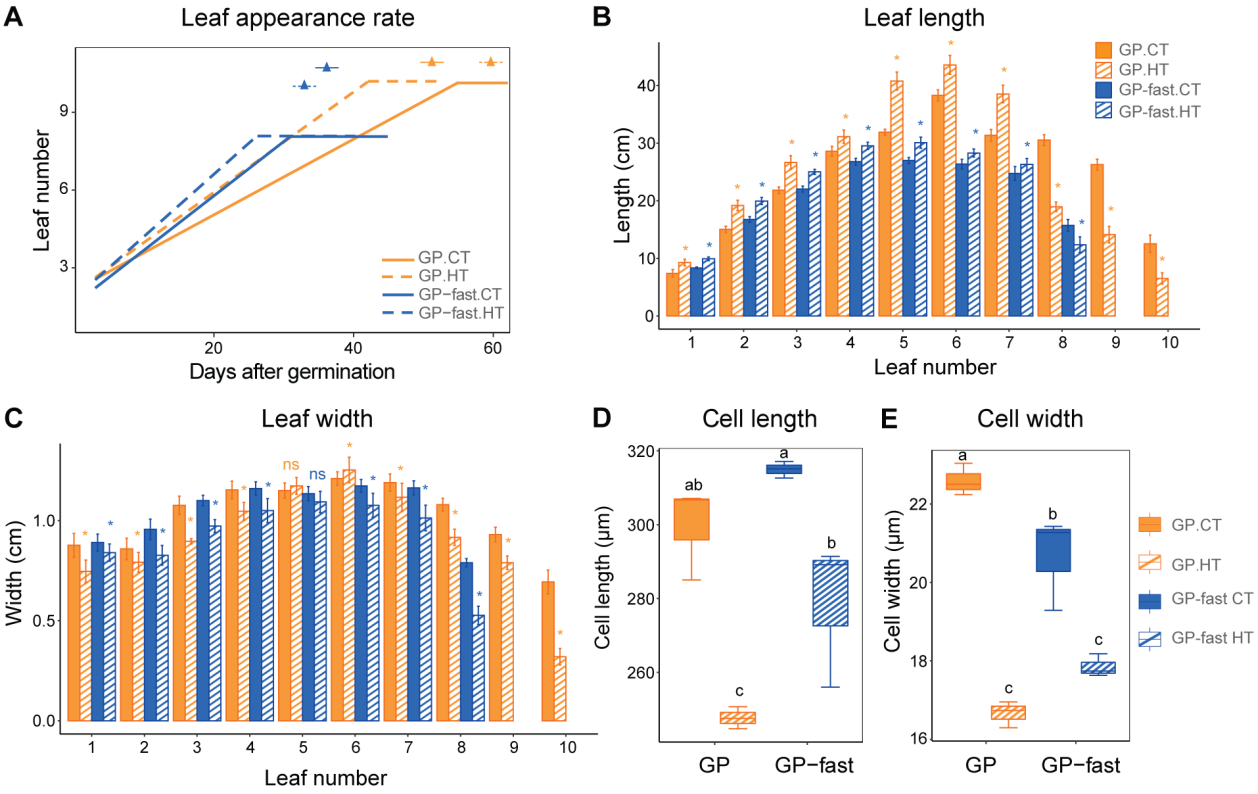

Figure S2. Effects of High Ambient Temperature on Leaf Development

Plants of spring barley cultivar Golden Promise (GP, *ppd-h1* allele) and its derived near-isogenic line GP-fast (*Ppd-H1* allele) were grown under long-day (16h/8h, day/night) under either control (CT; 20°C/16°C, day/night) or high ambient temperature (HT; 28°C/24°C, day/night) conditions. (A) Leaf appearance rate (LAR) was calculated as the time interval between the sequential emergence of leaves on the main culm (n = 15). The slope of the line indicates the LAR, and the symbol at the top of the graph indicates heading in days after germination (DAG). (B-C) Comparison of the leaf blade length (B) and width (C) of all leaves on the main culm of GP and GP-fast under CT and HT when the leaf was fully expanded (n = 15). (D-E) Comparison of cell length (D) and cell number (E) of the lateral cells from the adaxial epidermis of the 2nd leaf (L2) at 1/3 and 2/3 of leaf blade according to Wenzel et al. (1997) (n = 30). Error bars of the bar plots show the standard deviation. Box plots show the median and interquartile range. Whisker lines of box plots show the range of the minimum and maximum values. Statistical significance between CT and HT in each genotype was assessed using a two-tailed paired Student's t-test (ns indicates non-significant, * asterisks indicate $p < 0.05$). Statistical groups are assigned using ANOVA followed by Tukey's HSD test. Different letters indicate statistically significant differences between groups ($p < 0.05$).

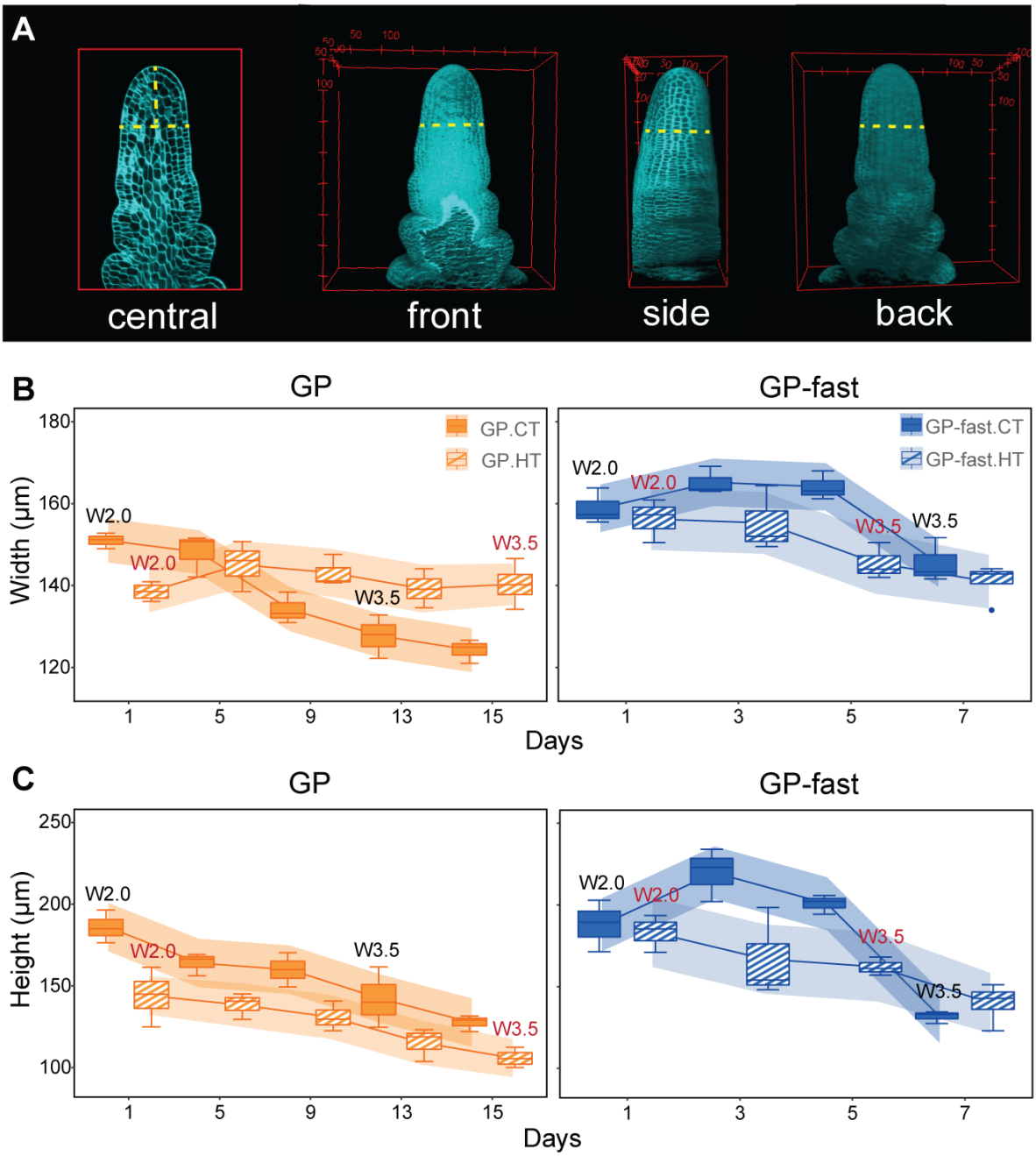

Figure S3. Effects of High Ambient Temperature on Inflorescence Meristem Size and Shape

(A) Confocal images of a representative inflorescence meristem (IM) at W2.0 to indicate the measurement of IM width (horizontal dashed line) and height (vertical dashed line). (B-D) Comparison of the width and height of IM in spring barley cultivar Golden Promise (GP, *ppd-h1* allele) and the derived near-isogenic line GP-fast (*Ppd-H1* allele) under long-day (16h/8h, day/night) control (CT; 20°C/16°C, day/night) and high ambient temperatures (HT; 28°C/24°C, day/night) (n = 3) during W2.0 to W3.5. Box plots show the median and interquartile range. Whisker lines of box plots show the range of the minimum and maximum values. Trend lines are calculated using a polynomial regression (Loess smooth line). Trend line areas show the 95% confidence interval.

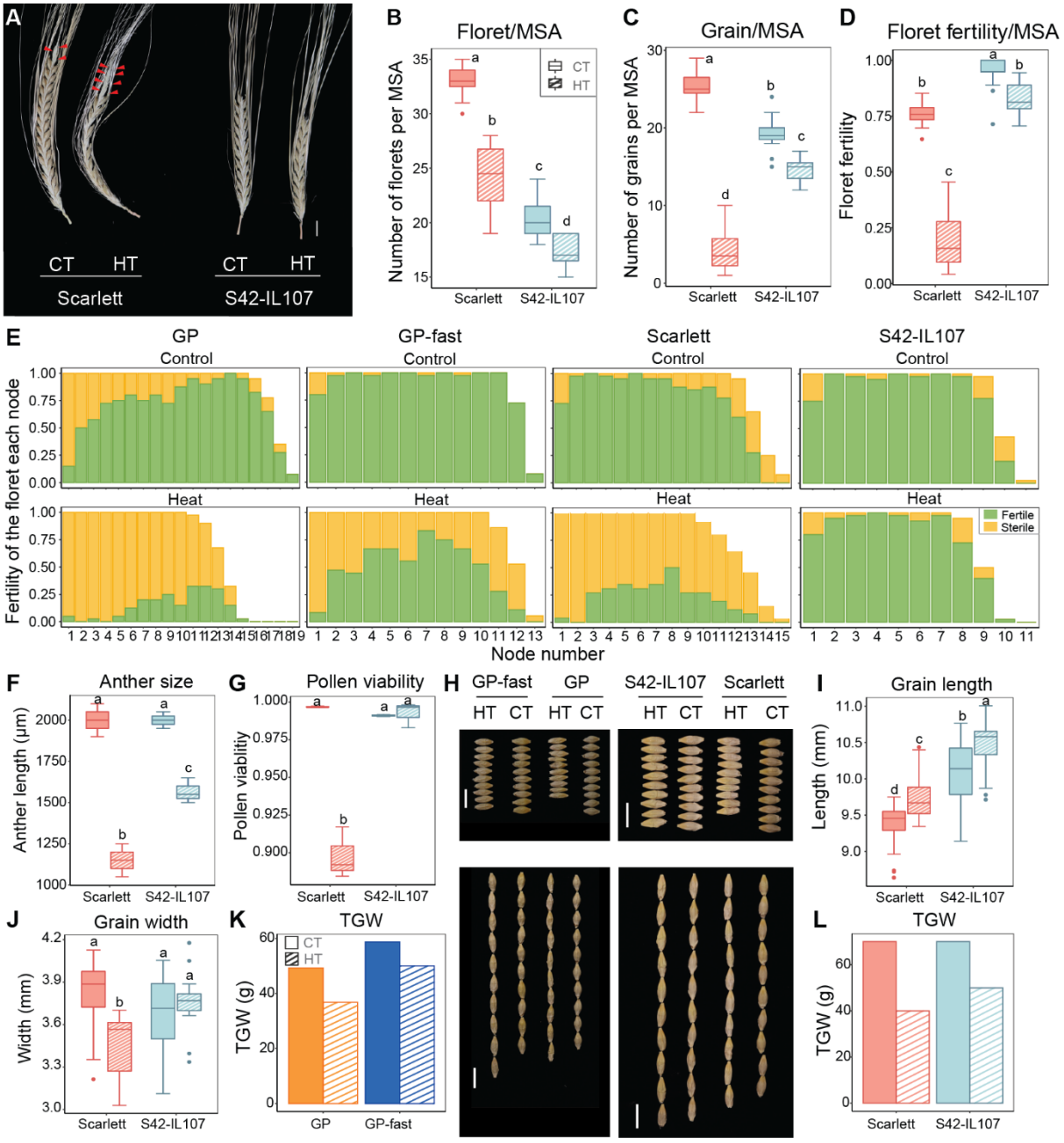

Figure S4. Effects of High Ambient Temperature on Floret Fertility and Grain Development in Scarlett and S42-IL107

(A) Main spike morphology of spring barley cultivar Scarlett (*ppd-h1* allele) and the derived near-isogenic line S42-IL107 (*Ppd-H1* allele), grown under long-day (16h/8h, day/night) either under control (CT; 20°C/16°C, day/night) or high ambient temperatures (HT; 28°C/24°C, day/night). Scale bar = 1 cm. The red triangles indicate the sterile florets. (B-D) Comparison of floret number, grain number, and floret fertility per main shoot apex (MSA) across genotype and treatment. (n = 11-15). Floret fertility was determined by the ratio of the grain number to the mature floret number. (E) Comparison of the floret fertility of each floret along the spike from the base (node 1) to the tip of the spike under CT and HT in each genotype. (n = 20). (F-G) Comparison of anther length and pollen viability from central florets at the middle of spike across genotype and treatment at W9.5 between CT and HT in Scarlett and S42-

IL107. (n = 3). (H) Grain morphology of spring barley Golden Promise (GP; *ppd-h1* allele) and Scarlett (*ppd-h1* allele), and their derived near-isogenic line GP-fast (*Ppd-H1* allele) and S42-IL107 (*Ppd-H1* allele) under CT and HT. Scale bar = 1 cm. (I-J) Comparison of grain length and width across genotype and treatment. (n = 30). (K-L) Comparison of thousand-grain weight (TGW) between GP and GP-fast and between Scarlett and S42-IL107 across treatment. Box plots show the median and interquartile range. Statistical groups are assigned using ANOVA followed by Tukey's HSD test. Different letters indicate statistically significant differences between groups ($p<0.05$).

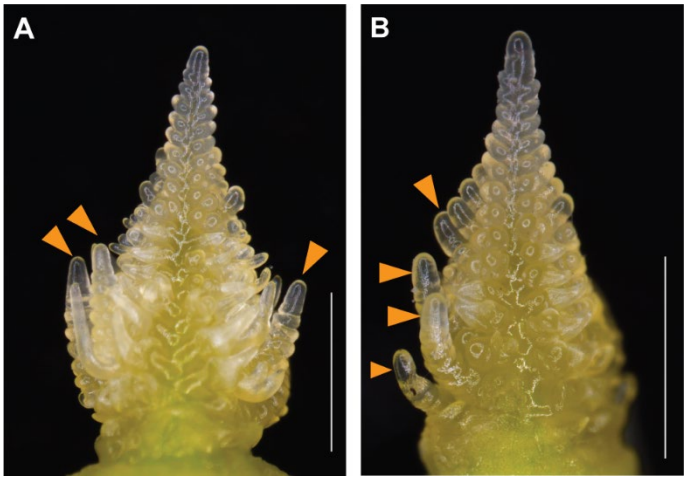

Figure S5. High Ambient Temperature before Spikelet initiation Causes Floral Reversion of the Spike of Golden Promise under High Ambient Temperature under Short-Day

(A-B) The morphology of the main shoot spike (MSA) of spring barley cultivar Golden Promise (GP, *ppd-h1*) grown under long-day (16h/8h, day/night) high ambient temperature (HT; 28°C/24°C, day/night) from germination to the spikelet induction stage (W2.0) and transferred to short-day (10h/14h, day/night) HT, referred to as HH. Scale bar = 1000 µm. The orange triangles indicate the floral reversion sites, where the floral meristem reversed into inflorescence meristems.

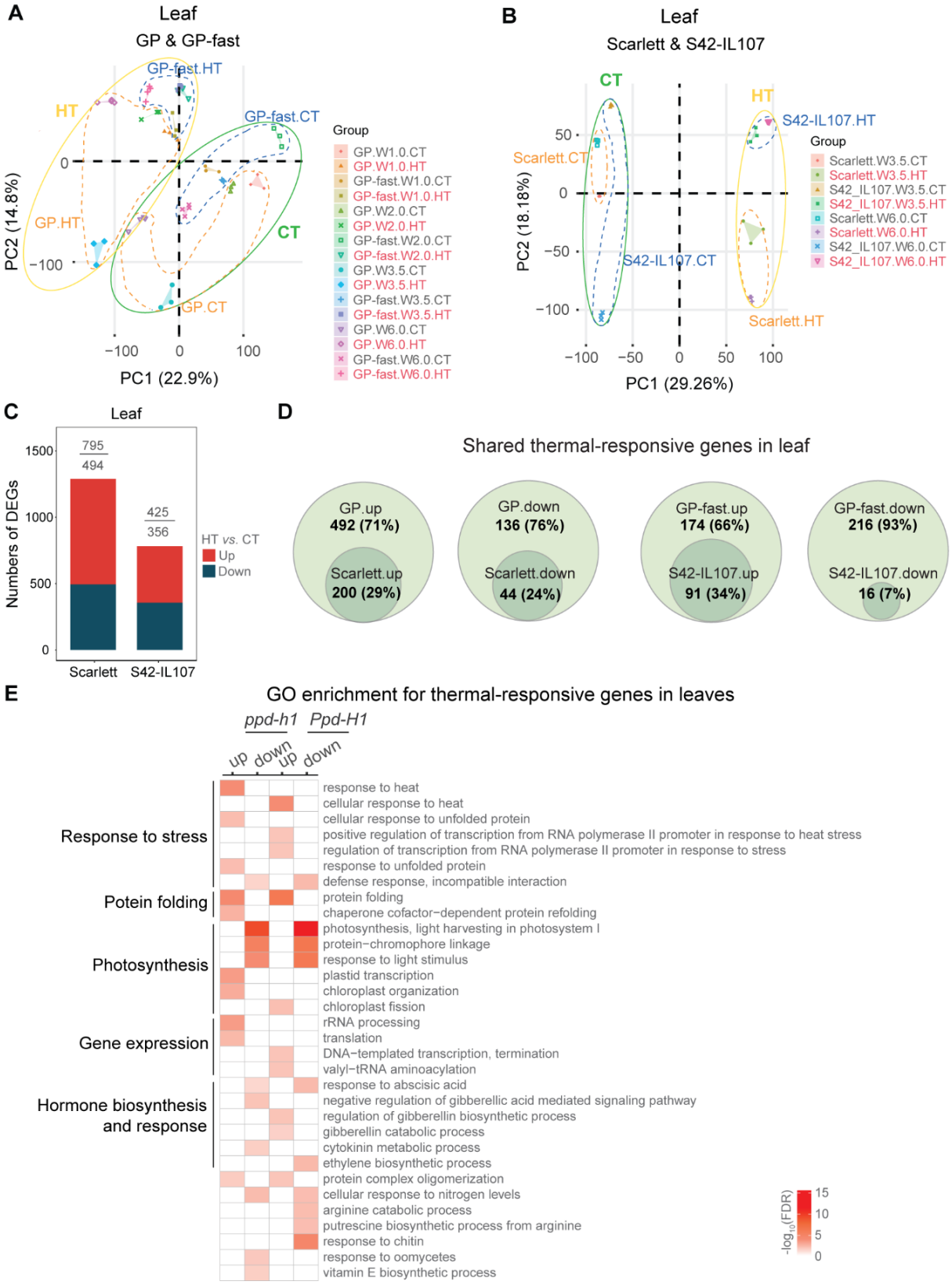

Figure S6. Thermal-Transcriptome Reprogramming in the Leaf

(A) The principal component analysis (PCA) of the leaf transcriptome of spring barley cultivar Golden Promise (GP; *ppd-h1* allele) and its derived near-isogenic line GP-fast (*Ppd-H1* allele) under long-day

(LD; 16h/8h, day/night) control (CT; 20°C/16°C, day/night) and high ambient temperatures (HT; 28°C/24°C, day/night) throughout vegetative (W1.0), early reproductive (W2.0 and W3.5) and late reproductive (W6.0) stages. (B) The PCA of the leaf transcriptome of Scarlett (*ppd-h1* allele) and its derived near-isogenic line S42-IL107 (*Ppd-H1* allele) under LD under CT and HT at W3.5 and W6.0. (C) Total number of differentially expressed genes (DEGs) in the leaf of Scarlett and S42-IL107. Red bars represent up-regulated DEGs (BH.FDR < 0.01, $\log_2$FC ≥ 1) and dark blue bars represent down-regulated DEGs (BH.FDR < 0.01, $\log_2$FC ≤ -1). (D) Gene Ontology (GO) analysis of the up- and down-regulated DEGs in leaf samples in response to HT shared between GP and Scarlett and between GP-fast and S42-IL107. For details, see the Methods and Supplemental Data (Table S4).

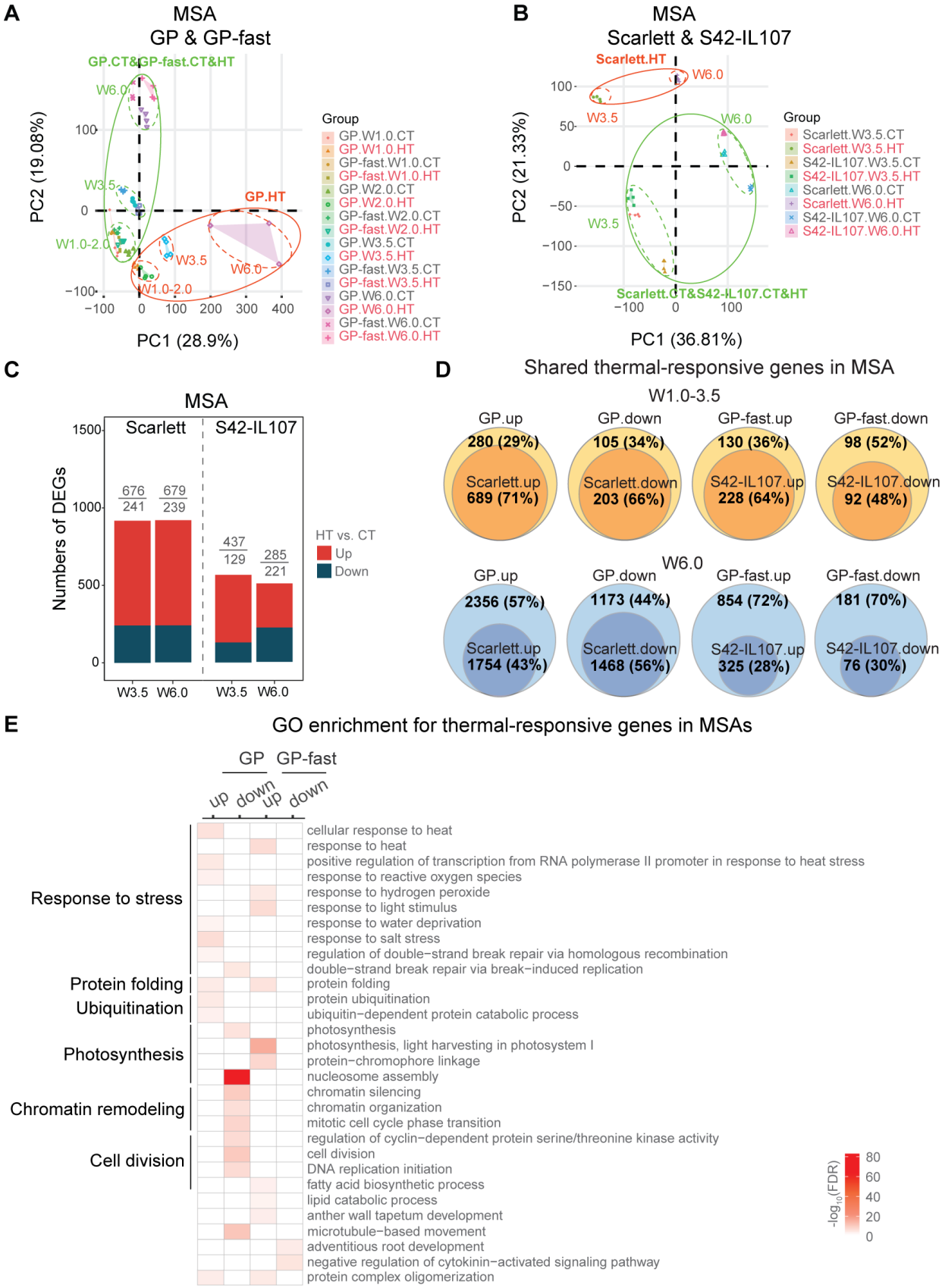

Figure S7. Thermal-Transcriptome Reprogramming in Main Shoot Apex

(A) The principal component analysis (PCA) of the main shoot apex (MSA) transcriptomes of spring barley cultivar Golden Promise (GP; *ppd-h1* allele) and its derived near-isogenic line GP-fast (*Ppd-H1*

allele) at long-day (LD, 16h/8h, day/night) under control (CT; 20°C/16°C, day/night) and high ambient temperature (HT; 28°C/24°C, day/night) throughout vegetative (W1.0), early reproductive (W2.0 and W3.5) and late reproductive (W6.0) stages. (B) The PCA of MSA transcriptomes of spring barley Scarlett (*ppd-h1* allele) and its derived near-isogenic line S42-IL107 (*Ppd-H1* allele) under LD under CT and HT at W3.5 and W6.0. (C) The number of differentially expressed genes (DEGs) in the MSA of Scarlett and S42-IL107 at W3.5 and W6.0, respectively. Red bars represent up-regulated DEGs (BH.FDR < 0.01, $\log_2$FC ≥ 1) and dark blue bars represent down-regulated DEGs (BH.FDR < 0.01, $\log_2$FC ≤ -1). (D) Gene Ontology (GO) analysis of the up- and down-regulated DEGs in the MSA in response to HT in GP and GP-fast. For details, see the Methods and Supplemental Data (Table S4).

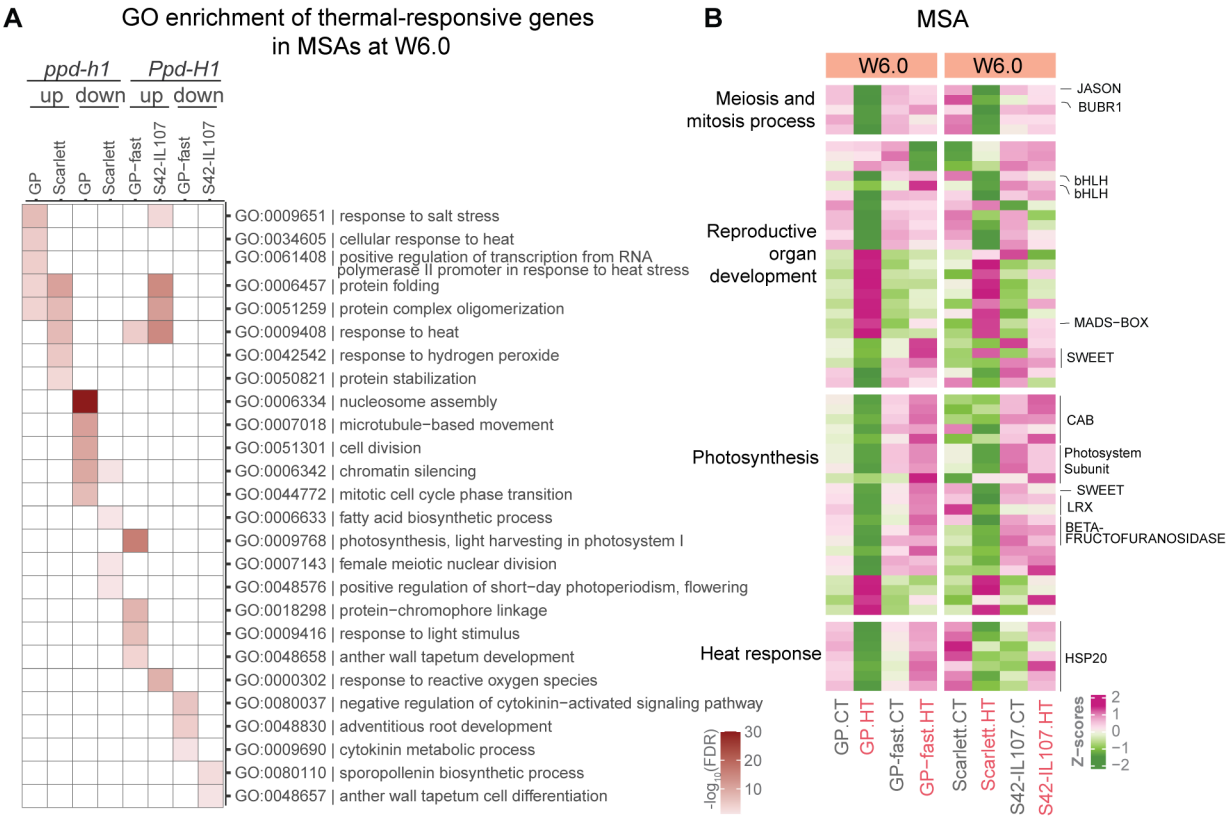

Figure S8. Differential Gene Expression Analysis in the Main Shoot Apex at Floral Development (W6.0)

(A) Gene ontology (GO) analysis of the differentially expressed genes (DEGs) in response to HT in the main shoot apex (MSA) at W6.0 shared between spring barley cultivars Golden Promise (GP; *ppd-h1* allele) and Scarlett (*ppd-h1* allele), and between their respective near-isogenic lines, GP-fast (*Ppd-H1* allele) and S42-IL107 (*Ppd-H1* allele). For details, see the Methods and Supplemental Data (Table S4). (B) The heatmap represents the transcript levels of DEGs from significant GO-enriched terms shown in A. The color scale represents the Z-score values of transcripts per million (TPM).

Table S1. Effects of High Ambient Temperature on Grain Set and Spikelet and Floral Meristem Induction under Long-Day.

Table S1. Effect of high ambient temperature on grain set and spikelet and floral meristem induction.

Traits	Stage	GP-fast (*Ppd-H1*)			GP (*ppd-h1*)			S42-IL107 (*Ppd-H1*)			Scarlett (*ppd-h1*)		
		CT	HT	*p*	CT	HT	*p*	CT	HT	*p*	CT	HT	*p*
Number of SMs	W2.0	14 ±1	15 ±1	**	18 ±1	19 ±1	*	14 ±1	14 ±1	ns	20 ±1	20 ±2	ns
	W3.5	26 ±1	27 ±1	ns	39 ±2	31 ±2	****	24 ±1	25 ±1	*	35 ±2	33 ±2	*
	W4.5	31 ±1	31 ±1	ns	43 ±2	35 ±1	****	31 ±1	29 ±2	***	40 ±1	39 ±2	*
	W6.0	34 ±1	30 ±1	****	43 ±2	36 ±2	****	32 ±1	29 ±2	*	42 ±2	41 ±1	**
Number of FMs	W3.5	9 ±2	10 ±2	ns	17 ±3	11 ±3	****	11 ±2	12 ±1	ns	18 ±4	13 ±4	**
	W4.5	20 ±1	25 ±4	****	31 ±2	27 ±6	*	21 ±2	23 ±2	**	35 ±1	35 ±3	ns
	W6.0	31 ±1	29 ±1	***	40 ±2	35 ±2	****	27 ±1	28 ±2	ns	39 ±2	40 ±1	ns
Duration (day)	W2.0-3.5	8	6		12	13		5	4		8	10	
	W3.5-4.5	5	4		4	8		4	3		6	6	
	W4.5-6.0	5	4		10	14		4	3		9	9	
Rate of SM initiation (SM / day)	W2.0-3.5	1.5	2.0		1.7	0.9		2.0	2.8		1.9	1.3	
	W3.5-4.5	1.0	1.1		1.1	0.6		1.7	1.1		0.8	0.9	
	W4.5-6.0	0.6	0.0		0.0	0.0		0.2	0.1		0.2	0.2	
Rate of FM initiation (FM / day)	W2.0-3.5	1.2	1.7		1.4	0.8		2.2	2.9		2.3	1.3	
	W3.5-4.5	2.8	5.0		3.4	2.1		2.6	4.0		2.8	3.7	
	W4.5-6.0	2.1	1.1		1.0	0.5		1.4	1.4		0.5	0.5	
Number of florets	matured	21 ±2	19 ±3	**	30 ±2	22 ±3	****	20 ±2	17 ±1	****	33 ±1	24 ±3	****
Number of grains	matured	20 ±2	15 ±2	****	24 ±3	5 ±3	****	19 ±2	15 ±2	****	25 ±2	5 ±3	****
Fertility (grains / florets)		1.0 ±0	0.8 ±0.1	****	0.8 ±0.1	0.2 ±0.1	****	0.9 ±0.1	0.8 ±0.1	***	0.8 ±0.1	0.2 ±0.1	****
Florets / SMs		0.6	0.6		0.7	0.6		0.6	0.6		0.8	0.6	
Grains / SMs		0.6	0.5		0.5	0.1		0.6	0.5		0.6	0.1	
Florets / FMs		0.7	0.6		0.7	0.6		0.8	0.6		0.8	0.6	
Grains / FMs		0.6	0.5		0.6	0.2		0.7	0.5		0.6	0.1	

Statistic test: Student T test, the pairwise comparisons are conducted within control and high ambient temperature in GP-fast, GP, Scarlett, and S42-IL107, respectively.
p value: $p > 0.05$ (ns); $p \leq 0.05$ (*); $p \leq 0.01$ (**); $p \leq 0.001$ (***); $p \leq 0.0001$ (***)
CT: control ambient temperature (20°C/16°C, day/night)
HT: high ambient temperature (28°C/24°C, day/night)
SM: spikelet meristem
FM: floral meristem

.

Table S2. Association Between Inflorescence Meristem Size and Spikelet Induction Rate.

Traits	Stage	GP (*ppd-h1*)		GP-fast (*Ppd-H1*)	
		CT	HT	CT	HT
IM height (μm)	W2.0	186 ±10 (a)	144 ±15 (b)	188 ±16 (a)	183 ±11 (a)
	W3.5	142 ±19 (b)	106 ±5 (c)	132 ±4 (bc)	162 ±6 (ab)
IM width (μm)	W2.0	151 ±2 (abc)	139 ±2 (de)	159 ±4 (a)	156 ±5 (ab)
	W3.5	128 ±5 (e)	140 ±5 (cd)	146 ±5 (bcd)	146 ±4 (bcd)
Rate of IM height decline (μm/day)	W2.0-3.5	3.7	2.7	9.4	5.3
Rate of IM width decline (μm/day)	W2.0-3.5	1.9	-0.1	2.2	2.7
Rate of SM initiation (SM/day)	W2.0-3.5	1.4	0.8	1.2	1.7

Statistic test: Tukey's HSD test, the pairwise comparisons are conducted across genotype and developmental stage.

Statistical significance: alpha = 0.05

CT: control ambient temperature (20°C/16°C, day/night)

HT: high ambient temperature (28°C/24°C, day/night)

IM: inflorescence meristem

SM: spikelet meristem

Table S3. RNAseq Analysis of Gene Expression in Leaves.

Table S4. GO Enrichment of Thermal-Responsive Genes in Leaves and Main Shoot Apices.

Table S5. GO Enrichment of Genes Differentially Expressed between Parental Lines and Near-Isogenic Lines in Leaves and Main Shoot Apices.

Table S6. RNAseq Analysis of Gene Expression in Main Shoot Apices.

Table S7. Sequencing Details.

Table S3. S4. S5, S6, and S7 can be downloaded from the link:

https://www.dropbox.com/scl/fo/zwh86usy4216lb3jsdg7r/AFDNaJ-LxpkN3Lmj3s2428A?rlkey=qip3qvn651r8s1yw7u916s03f&st=t3pks8nx&dl=0

Table S8. Primers Used in This Study

Usage	Name	Sequence 5'-3'
qRT-PCR	VRT2-F	CCGATGTTGTCCCTGAAGAT
	VRT2-R	GGAACTCCCTCATGGACTCA
	BM1-F	AGAGGAGAACGCAAGGCTAAAGG
	BM1-R	AGTTGAAGAGTGATAATCCGAGCCTGAG
	BM10-F	GCTCATCGTCTTCTCCTCCAC
	BM10-R	CTCCTCGCCTCTCATCTGTC
	CEN-F	TTTGGAAGGGAGGTGGTGAG
	CEM-R	GAAGTAGACGGCAGCGACAG
	ACTIN-F	CGTGTTGGATTCTGGTGATG
	ACTIN-R	AGCCACATATGCGAGCTTCT
RNA *in situ* hybridization	FT2-T3-F1	ATTAACCCTCACTAAAGGGAGGATGTGATGATCGACTCCTTG
	FT2-T7-R1	TAATACGACTCACTATAGGGGGACAATCTCAAGCACCCAAG
	FT2-T3-F2	ATTAACCCTCACTAAAGGGAGGTCGTATGGGTGGTTTATACG
	FT2-T7-R2	TAATACGACTCACTATAGGGCCAGAAGAGACAGCCACCTTG
	FPFL-T3-F1	ATTAACCCTCACTAAAGGGACGCATGTCTACGAGTAAGCG
	FPFL-T7-R1/2	TAATACGACTCACTATAGGGGTGTCCTGTGGTCAATGCTG
	FPFL-T3-F2	ATTAACCCTCACTAAAGGGAGGTTAGCTAGTGTCGGCTGTAG

7 References

Abiko, M., Akibayashi, K., Sakata, T., Kimura, M., Kihara, M., Itoh, K., Asamizu, E., Sato, S., Takahashi, H., and Higashitani, A. (2005). High-temperature induction of male sterility during barley (*Hordeum vulgare* L.) anther development is mediated by transcriptional inhibition. Sex Plant Reproduction **18**, 91-100.

Abou-Elwafa, S.F., and Amein, K.A. (2016). Genetic diversity and potential high temperature tolerance in barley (*Hordeum vulgare*). World Journal of Agricultural Research **4**, 1-8.

Backhaus, A.E., Lister, A., Tomkins, M., Adamski, N.M., Simmonds, J., Macaulay, I., Morris, R.J., Haerty, W., and Uauy, C. (2022). High expression of the MADS-box gene VRT2 increases the number of rudimentary basal spikelets in wheat. Plant Physiology **189**, 1536-1552.

Balasubramanian, S., Sureshkumar, S., Lempe, J., and Weigel, D. (2006). Potent induction of Arabidopsis thaliana flowering by elevated growth temperature. PLoS Genetics **2**, e106.

Batts, G., Morison, J., Ellis, R., Hadley, P., and Wheeler, T. (1997). Effects of CO2 and temperature on growth and yield of crops of winter wheat over four seasons. European Journal of Agronomy **7**, 43-52.

Bi, X., van Esse, W., Mulki, M.A., Kirschner, G., Zhong, J., Simon, R., and von Korff, M. (2019). CENTRORADIALIS interacts with FLOWERING LOCUS T-like genes to control floret development and grain number. Plant physiology **180**, 1013-1030.

Bommert, P., and Whipple, C. (2018). Grass inflorescence architecture and meristem determinacy. In Seminars in Cell & Developmental Biology (Elsevier), **79**, 37-47.

Bommert, P., Nagasawa, N.S., and Jackson, D. (2013). Quantitative variation in maize kernel row number is controlled by the FASCIATED EAR2 locus. Nature Genetics **45**, 334-337.

Bonnett, O.T. (1966). Inflorescences of maize, wheat, rye, barley, and oats: their initiation and development. Bulletin (University of Illinois (Urbana-Champaign campus). Agricultural Experiment Station); no. 721.

Casal, J.J., and Balasubramanian, S. (2019). Thermomorphogenesis. Annual Review of Plant Biology **70**, 321-346.

Chen, Y., Song, W., Xie, X., Wang, Z., Guan, P., Peng, H., Jiao, Y., Ni, Z., Sun, Q., and Guo, W. (2020). A collinearity-incorporating homology inference strategy for connecting emerging assemblies in the triticeae tribe as a pilot practice in the plant pangenomic era. Molecular Plant **13,** 1694-1708.

Chu, H., Qian, Q., Liang, W., Yin, C., Tan, H., Yao, X., Yuan, Z., Yang, J., Huang, H., and Luo, D. (2006). The floral organ number4 gene encoding a putative

ortholog of Arabidopsis CLAVATA3 regulates apical meristem size in rice. Plant Physiology **142**, 1039-1052.

Crawford, A.J., McLachlan, D.H., Hetherington, A.M., and Franklin, K.A. (2012). High temperature exposure increases plant cooling capacity. Current Biology **22**, R396-R397.

De Mendiburu, F. (2021). Agricolae tutorial (Version 1.3-5). Universidad Nacional Agraria: La Molina, Peru.

Delker, C., Quint, M., and Wigge, P.A. (2022). Recent advances in understanding thermomorphogenesis signaling. Current Opinion in Plant Biology **68,** 102231.

Digel, B., Pankin, A., and von Korff, M. (2015). Global Transcriptome Profiling of Developing Leaf and Shoot Apices Reveals Distinct Genetic and Environmental Control of Floral Transition and Inflorescence Development in Barley. The Plant Cell **27,** 2318-2334.

Dixon, L.E., Karsai, I., Kiss, T., Adamski, N.M., Liu, Z., Ding, Y., Allard, V., Boden, S.A., and Griffiths, S. (2019). VERNALIZATION1 controls developmental responses of winter wheat under high ambient temperatures. Development **146,** dev172684.

Ejaz, M., and von Korff, M. (2017). The Genetic Control of Reproductive Development under High Ambient Temperature. Plant Physiology **173,** 294-306.

Ewels, P., Magnusson, M., Lundin, S., and Käller, M. (2016). MultiQC: summarize analysis results for multiple tools and samples in a single report. Bioinformatics **32**, 3047-3048.

Franklin, K.A., Lee, S.H., Patel, D., Kumar, S.V., Spartz, A.K., Gu, C., Ye, S., Yu, P., Breen, G., and Cohen, J.D. (2011). Phytochrome-interacting factor 4 (PIF4) regulates auxin biosynthesis at high temperature. Proceedings of the National Academy of Sciences **108**, 20231-20235.

Gol, L., Haraldsson, E.B., and von Korff, M. (2021). Ppd-H1 integrates drought stress signals to control spike development and flowering time in barley. Journal of Experimental Botany **72**, 122-136.

Gray, W.M., Östin, A., Sandberg, G., Romano, C.P., and Estelle, M. (1998). High temperature promotes auxin-mediated hypocotyl elongation in Arabidopsis. Proceedings of the National Academy of Sciences **95**, 7197-7202.

Guo, W., Tzioutziou, N.A., Stephen, G., Milne, I., Calixto, C.P., Waugh, R., Brown, J.W., and Zhang, R. (2021). 3D RNA-seq: a powerful and flexible tool for rapid and accurate differential expression and alternative splicing analysis of RNA-seq data for biologists. RNA Biology **18**, 1574-1587.

Hakala, K., Jauhiainen, L., Himanen, S., Rötter, R., Salo, T., and Kahiluoto, H. (2012). Sensitivity of barley varieties to weather in Finland. The Journal of Agricultural Science **150**, 145-160.

Heisler, M.G., Ohno, C., Das, P., Sieber, P., Reddy, G.V., Long, J.A., and Meyerowitz, E.M. (2005). Patterns of auxin transport and gene expression

during primordium development revealed by live imaging of the Arabidopsis inflorescence meristem. Current Biology **15**, 1899-1911.

Hemming, M.N., Walford, S.A., Fieg, S., Dennis, E.S., and Trevaskis, B. (2012). Identification of high-temperature-responsive genes in cereals. Plant Physiology **158**, 1439-1450.

Huai, J., Zhang, X., Li, J., Ma, T., Zha, P., Jing, Y., and Lin, R. (2018). SEUSS and PIF4 coordinately regulate light and temperature signaling pathways to control plant growth. Molecular plant **11**, 928-942.

Huang, Y., Kamal, R., Shanmugaraj, N., Rutten, T., Thirulogachandar, V., Zhao, S., Hoffie, I., Hensel, G., Rajaraman, J., and Moya, Y.A.T. (2023). A molecular framework for grain number determination in barley. Science Advances **9**, eadd0324.

Intergovernmental Panel on Climate (IPCC) (2023). Climate Change 2022 – Impacts, Adaptation and Vulnerability.

Kirschner, G.K., Stahl, Y., Imani, J., von Korff, M., and Simon, R. (2018). Fluorescent reporter lines for auxin and cytokinin signalling in barley *(Hordeum vulgare*). PLoS One **13**, e0196086.

Kiss, T., Dixon, L.E., Soltész, A., Bányai, J., Mayer, M., Balla, K., Allard, V., Galiba, G., Slafer, G.A., and Griffiths, S. (2017). Effects of ambient temperature in association with photoperiod on phenology and on the expressions of major plant developmental genes in wheat (*Triticum aestivum* L.). Plant, Cell & Environment **40**, 1629-1642.

Koini, M.A., Alvey, L., Allen, T., Tilley, C.A., Harberd, N.P., Whitelam, G.C., and Franklin, K.A. (2009). High temperature-mediated adaptations in plant architecture require the bHLH transcription factor PIF4. Current Biology **19**, 408-413.

Kumar, S.V., Lucyshyn, D., Jaeger, K.E., Alós, E., Alvey, E., Harberd, N.P., and Wigge, P.A. (2012). Transcription factor PIF4 controls the thermosensory activation of flowering. Nature **484**, 242-245.

Kurihara, D., Mizuta, Y., Sato, Y., and Higashiyama, T. (2015). ClearSee: a rapid optical clearing reagent for whole-plant fluorescence imaging. Development **142**, 4168-4179.

Langridge, P. (2018). Economic and academic importance of barley. The barley genome, 1-10.

Li, S., Meng, S., Weng, J., and Wu, Q. (2022). Fine-tuning shoot meristem size to feed the world. Trends in Plant Science **27**, 355-363.

Liu, B., Asseng, S., Müller, C., Ewert, F., Elliott, J., Lobell, D.B., Martre, P., Ruane, A.C., Wallach, D., and Jones, J.W. (2016). Similar estimates of temperature impacts on global wheat yield by three independent methods. Nature Climate Change **6**, 1130-1136.

Liu, T., Carlsson, J., Takeuchi, T., Newton, L., and Farre, E.M. (2013). Direct regulation of abiotic responses by the A rabidopsis circadian clock component PRR 7. The Plant Journal **76**, 101-114.

Liu, Z., Xin, M., Qin, J., Peng, H., Ni, Z., Yao, Y., and Sun, Q. (2015). Temporal transcriptome profiling reveals expression partitioning of homeologous genes contributing to heat and drought acclimation in wheat (*Triticum aestivum* L.). BMC Plant Biology **15**, 1-20.

Livak, K.J., and Schmittgen, T.D. (2001). Analysis of Relative Gene Expression Data Using Real-Time Quantitative PCR and the 2−ΔΔCT Method. Methods **25**, 402-408.

Lobell, D.B., Schlenker, W., and Costa-Roberts, J. (2011). Climate trends and global crop production since 1980. Science **333,** 616-620.

Mahalingam, R., Duhan, N., Kaundal, R., Smertenko, A., Nazarov, T., and Bregitzer, P. (2022). Heat and drought induced transcriptomic changes in barley varieties with contrasting stress response phenotypes. Frontiers in Plant Science **13**, 1066421.

Mansour, E., Casas, A.M., Gracia, M.P., Molina-Cano, J.L., Moralejo, M., Cattivelli, L., Thomas, W.T., and Igartua, E. (2014). Quantitative trait loci for agronomic traits in an elite barley population for Mediterranean conditions. Molecular Breeding **33**, 249-265.

Mascher, M., Wicker, T., Jenkins, J., Plott, C., Lux, T., Koh, C.S., Ens, J., Gundlach, H., Boston, L.B., and Tulpová, Z. (2021). Long-read sequence assembly: a technical evaluation in barley. The Plant Cell **33**, 1888-1906.

Mikołajczak, K., Kuczyńska, A., Krajewski, P., Kempa, M., and Nuc, M. (2023). Transcriptome profiling disclosed the effect of single and combined drought and heat stress on reprogramming of genes expression in barley flag leaf. Frontiers in Plant Science **13**, 1096685.

Musielak, T.J., Schenkel, L., Kolb, M., Henschen, A., and Bayer, M. (2015). A simple and versatile cell wall staining protocol to study plant reproduction. Plant Reproduction **28**, 161-169.

Nelissen, H., Gonzalez, N., and Inze, D. (2016). Leaf growth in dicots and monocots: so different yet so alike. Current Opinion in Plant Biology **33**, 72-76.

Ottman, M., Kimball, B., White, J., and Wall, G. (2012). Wheat growth response to increased temperature from varied planting dates and supplemental infrared heating. Agronomy Journal **104**, 7-16.

Patro, R., Duggal, G., Love, M.I., Irizarry, R.A., and Kingsford, C. (2017). Salmon provides fast and bias-aware quantification of transcript expression. Nature Methods **14**, 417-419.

Peterson, R., Slovin, J.P., and Chen, C. (2010). A simplified method for differential staining of aborted and non-aborted pollen grains. International Journal of Plant Biology **1**, e13.

Qin, D., Wu, H., Peng, H., Yao, Y., Ni, Z., Li, Z., Zhou, C., and Sun, Q. (2008). Heat stress-responsive transcriptome analysis in heat susceptible and tolerant wheat (Triticum aestivum L.) by using Wheat Genome Array. BMC genomics **9,** 1-19.

R Core Team, R. (2013). R: A language and environment for statistical computing.

Rapazote-Flores, P., Bayer, M., Milne, L., Mayer, C.-D., Fuller, J., Guo, W., Hedley, P.E., Morris, J., Halpin, C., and Kam, J. (2019). BaRTv1. 0: an improved barley reference transcript dataset to determine accurate changes in the barley transcriptome using RNA-seq. BMC Genomics **20**, 1-17.

Reinhardt, D., Mandel, T., and Kuhlemeier, C. (2000). Auxin regulates the initiation and radial position of plant lateral organs. The Plant Cell **12**, 507-518.

Robinson, M.D., McCarthy, D.J., and Smyth, G.K. (2010). edgeR: a Bioconductor package for differential expression analysis of digital gene expression data. bioinformatics **26**, 139-140.

Sakata, T., Oshino, T., Miura, S., Tomabechi, M., Tsunaga, Y., Higashitani, N., Miyazawa, Y., Takahashi, H., Watanabe, M., and Higashitani, A. (2010). Auxins reverse plant male sterility caused by high temperatures. Proceedings of the National Academy of Sciences **107,** 8569-8574.

Sang, Q., Pajoro, A., Sun, H., Song, B., Yang, X., Stolze, S.C., Andrés, F., Schneeberger, K., Nakagami, H., and Coupland, G. (2020). Mutagenesis of a quintuple mutant impaired in environmental responses reveals roles for CHROMATIN REMODELLING4 in the Arabidopsis floral transition. The Plant Cell **32**, 1479-1500.

Schindelin, J., Arganda-Carreras, I., Frise, E., Kaynig, V., Longair, M., Pietzsch, T., Preibisch, S., Rueden, C., Saalfeld, S., and Schmid, B. (2012). Fiji: an open-source platform for biological-image analysis. Nature Methods **9**, 676-682.

Schmalenbach, I., March, T.J., Bringezu, T., Waugh, R., and Pillen, K. (2011). High-resolution genotyping of wild barley introgression lines and fine-mapping of the threshability locus thresh-1 using the Illumina GoldenGate assay. G3: Genes| Genomes| Genetics **1**, 187-196.

Shavrukov, Y., Kurishbayev, A., Jatayev, S., Shvidchenko, V., Zotova, L., Koekemoer, F., De Groot, S., Soole, K., and Langridge, P. (2017). Early flowering as a drought escape mechanism in plants: how can it aid wheat production? Frontiers in Plant Science **8**, 1950.

Shi, B., Guo, X., Wang, Y., Xiong, Y., Wang, J., Hayashi, K.-i., Lei, J., Zhang, L., and Jiao, Y. (2018). Feedback from lateral organs controls shoot apical meristem growth by modulating auxin transport. Developmental Cell **44**, 204-216. e206.

Slafer, G.A., Casas, A.M., and Igartua, E. (2023). Sense in sensitivity: difference in the meaning of photoperiod-insensitivity between wheat and barley. Journal of Experimental Botany**,** erad128.

Suzaki, T., Toriba, T., Fujimoto, M., Tsutsumi, N., Kitano, H., and Hirano, H.-Y. (2006). Conservation and diversification of meristem maintenance mechanism in Oryza sativa: function of the FLORAL ORGAN NUMBER2 gene. Plant and Cell Physiology **47**, 1591-1602.

Tashiro, T., and Wardlaw, I.F. (1989). A comparison of the effect of high temperature on grain development in wheat and rice. Annals of Botany **64**, 59-65.

Trevaskis, B., Tadege, M., Hemming, M.N., Peacock, W.J., Dennis, E.S., and Sheldon, C. (2007). Short vegetative phase-like MADS-box genes inhibit floral meristem identity in barley. Plant Physiology **143**, 225-235.

Turner, A., Beales, J., Faure, S., Dunford, R.P., and Laurie, D.A. (2005). The Pseudo-Response Regulator Ppd-H1 Provides Adaptation to Photoperiod in Barley **310**, 1031-1034.

Van Der Woude, L.C., Perrella, G., Snoek, B.L., Van Hoogdalem, M., Novák, O., Van Verk, M.C., Van Kooten, H.N., Zorn, L.E., Tonckens, R., and Dongus, J.A. (2019). HISTONE DEACETYLASE 9 stimulates auxin-dependent thermomorphogenesis in Arabidopsis thaliana by mediating H2A. Z depletion. Proceedings of the National Academy of Sciences **116**, 25343-25354.

van Zanten, M., Voesenek, L.A., Peeters, A.J., and Millenaar, F.F. (2009). Hormone-and light-mediated regulation of heat-induced differential petiole growth in Arabidopsis. Plant Physiology **151**, 1446-1458.

Waddington, S.R., Cartwright, P.M., and Wall, P.C. (1983). A quantitative scale of spike initial and pistil development in barley and wheat. Annals of Botany **51**, 119-130.

Wang, C., Yang, X., Zhang, Y., Shen, C., Shi, J., Xia, C., Fang, T., Tu, Q., Li, L., and Zhou, X. (2023). Barley FASCIATED EAR genes determine inflorescence meristem size and yield traits. The Crop Journal **11**, 679-691.

Wenzel, C.L., Chandler, P.M., Cunningham, R. B., and Passioura, J.B. (1997). Characterization of the Leaf Epidermis of Barley (Hordeum vulgareL.'Himalaya'). Annals of Botany **79**, 41-46.

Wiegmann, M., Maurer, A., Pham, A., March, T.J., Al-Abdallat, A., Thomas, W.T., Bull, H.J., Shahid, M., Eglinton, J., and Baum, M. (2019). Barley yield formation under abiotic stress depends on the interplay between flowering time genes and environmental cues. Scientific Reports **9,** 6397.

Xie, W., Xiong, W., Pan, J., Ali, T., Cui, Q., Guan, D., Meng, J., Mueller, N.D., Lin, E., and Davis, S.J. (2018). Decreases in global beer supply due to extreme drought and heat. Nature Plants **4**, 964-973.

Yamaguchi, N., Wu, M.-F., Winter, C.M., Berns, M.C., Nole-Wilson, S., Yamaguchi, A., Coupland, G., Krizek, B.A., and Wagner, D. (2013). A molecular framework for auxin-mediated initiation of flower primordia. Developmental Cell **24**, 271-282.

Yang, M., Han, X., Yang, J., Jiang, Y., and Hu, Y. (2021). The Arabidopsis circadian clock protein PRR5 interacts with and stimulates ABI5 to modulate abscisic acid signaling during seed germination. The Plant Cell **33**, 3022-3041.

Zadoks, J.C., Chang, T.T., and Konzak, C.F. (1974). A decimal code for the growth stages of cereals. Weed Research **14**, 415-421.

Zhang, X., Rerksiri, W., Liu, A., Zhou, X., Xiong, H., Xiang, J., Chen, X., and Xiong, X. (2013). Transcriptome profile reveals heat response mechanism at molecular and metabolic levels in rice flag leaf. Gene **530**, 185-192.

Zhang, X., Li, J., Liu, A., Zou, J., Zhou, X., Xiang, J., Rerksiri, W., Peng, Y., Xiong, X., and Chen, X. (2012). Expression profile in rice panicle: insights into heat response mechanism at reproductive stage. Plos One **7**, e49652.

Zhao, C., Liu, B., Piao, S., Wang, X., Lobell, D.B., Huang, Y., Huang, M., Yao, Y., Bassu, S., and Ciais, P. (2017). Temperature increase reduces global yields of major crops in four independent estimates. Proceedings of the National Academy of Sciences **114**, 9326-9331.

Zhu, Z., Esche, F., Babben, S., Trenner, J., Serfling, A., Pillen, K., Maurer, A., and Quint, M. (2023). An exotic allele of barley EARLY FLOWERING 3 contributes to developmental plasticity at elevated temperatures. Journal of Experimental Botany **74**, 2912-2931.

8 Abbreviations

Abbreviation	Explanation
ARC5	ACCUMULATION AND REPLICATION OF CHLOROPLAST 5
BLAST	Basic local alignment search tool
BLASTn	BLASTs with nucleotide query against a nucleotide database
BLASTx	BLASTs with nucleotide query against a translated nucleotide database
BM1/BM3/BM8/BM10	BARLEY MADS BOX 1/3/8/10
CAB	CHLOROPHYLL A/B BINDING
CC	Control ambient temperature before and after spikelet initiation
CCT-domain	CONSTANTS, CO-like, and TOC1-domain
CEN	CENTRORADIALIS
CH	Control ambient temperature before spikelet initiation but high ambient temperature after spikelet initiation
CT	Control ambient temperature
DAG	Days after germination
DRM/ARP	DORMANCY/AUXIN ASSOCIATED gene
FDR	False discovery rate
FM	Floral meristem
FPFL	FLOWERING PROMOTING FACTOR-LIKE
FT	FLOWERING LOCUS T
FT1/2/4	FLOWERING LOCUS T1/2/4
GO	Gene Ontology
GP	Golden Promise
GP-fast	Golden Promise-fast
HC	High ambient temperature before spikelet initiation and control ambient temperature after spikelet initiation
HH	High ambient temperature before and after spikelet initiation
HSF	HEAT SHOCK TRANSCRIPTION FACTOR
HSP	HEAT SHOCK PROTEIN
HT	High ambient temperature
IM	Inflorescence meristem
LD	Long-day
LRR-RLK	LEUCINE-RICH REPEAT RECEPTOR-LIKE KINASES
LRX	LEUCINE-RICH REPEAT EXTENSIN
MSA	Main shoot apex
NIL	Near-isogenic line
PIF4	PHYTOCHROME-INTERACTING FACTOR 4
PPD-H1, PPD1	PHOTOPERIOD 1
PRR37	PSEUDO RESPONSE REGULATOR 37
p-value	Probability value
RBCS1A	RIBULOSE BISPHOSPHATE CARBOXYLASE SMALL CHAIN 1A
RNA-seq	RNA-sequencing
SAM	Shoot apical meristem
SAUR-LIKE	SMALL AUXIN-UPREGULATED RNA-LIKE

Abbreviation	Explanation
SM	Spikelet meristem
SRS	SHI-RELATED SEQUENCE
SVP	SHORT VEGETATIVE PHASE
SWEET	SUGARS WILL EVENTUALLY BE EXPORTED TRANSPORTERS
TPM	Transcripts per million
VRN1	VERNALIZATION 1
VRT2	VEGETATIVE TO REPRODUCTIVE TRANSITION 2

9 Acknowledgements

No words can express my gratitude and appreciation for the people who have supported and assisted me during my Ph.D. I should thank each and every one of you for making this academic pursuit possible. It has been an invaluable chapter of my life.

My deepest thanks go to my supervisor, Maria von Korff Schmising, for her steadfast guidance and support. I am truly thankful for the opportunities you provided me to work on such an interesting project and for guiding me through the challenges to achieve success. Your cultivation has not only made me a better researcher but also shaped me to excel both in academia and personally.

I am extremely grateful to my second supervisor, Rüdiger Simon, for co-supervising my thesis. I am truly thankful for your insightful advices and generous support. The reporter lines you generated and shared with me have yielded valuable results for this work.

I would like to acknowledge the funding sources, China Scholarship Council (CSC) (for the first four years) and Heinrich-Heine-Universität Düsseldorf (HHU) (for the writing phase of my thesis), to make my Ph.D. work possible. Of course, I truly appreciate the funding support Maria has offered, allowing me to yield more creativity and results.

Special thanks go to Agatha, Einar, and Gesa for their tremendous support and assistance on scientific and non-scientific questions and for always being there for me. Your contributions were pivotal in the success of my research.

Thanks to all members of AG von Korff for fostering such a warm and welcoming working environment. It has made me feel like I have a second family here, and I am truly grateful for it. I would like to express my appreciation to our super technical and secretary team, Thea, Rebekka, Nina, Gabriele, and Bettina. Thank you for your tireless efforts in assisting me with my project and official matters, and taking care of my bushy and unhappy plants grown under the stress treatment. I would like to extend my gratitude to our former group member, Jinshun, for his experimental guidance and expertise on the RNA *in situ* hybridization and the 3D confocal imaging reconstruction, and to the HHU CAi team members, Sebastian and Stefanie, for their technical support on the confocal imaging.

I would like to extend my sincere thanks to all my friends. Your companionship has added vibrant colors and anticipation to my life and kept me energized and motivated. A special appreciation to Edgar, Isaia, Anika, and Jan. I am truly grateful for your inspiring discussions, collaborations, and moral support.

Lastly, I want to express my heartfelt appreciation to my love, Ruibin, and my amazing parents. You have always fueled my passion for science and supported me in everything I have pursued. It is your understanding and love that have developed me into who I am. 谢谢爸爸、妈妈和瑞斌的理解与爱，我爱你们!